AN ABSTRACT OF THE THESIS OF

Adrian Kidarsa for the degree of Master of Science in Civil Engineering presented on June 14, 2006.
Title: Analysis of Moving Loads Using Force-Based Finite Elements.

Abstract approved:

Redacted for privacy

Michael H. Scott

An analysis method for moving loads computes the internal demand history in a structural member at integration points of force-based finite elements as opposed to the end forces of a refined displacement-based finite element mesh. The force-based formulation satisfies strong equilibrium of internal section forces with the element end forces and the moving load. This is in contrast with the displacement-based finite element formulations that violate equilibrium between the section forces and the equivalent end forces computed for the moving load. A new approach to numerical quadrature in force-based elements allows the specification of integration point locations, where the section demand history is critical, while ensuring a sufficient level of integration accuracy over the element domain. Influence lines computed by numerical integration in force-based elements converge to the exact solution. Accurate results are obtained for practical applications in structural engineering through the low-order integration approach.

Analysis of Moving Loads Using Force-Based Finite Elements

by
Adrian Kidarsa

A THESIS

submitted to

Oregon State University

in partial fulfillment of
the requirements for the
degree of

Master of Science

Presented June 14, 2006
Commencement June 2007

Master of Science thesis of Adrian Kidarsa presented on June 14, 2006.

APPROVED:

Redacted for privacy

Major Professor, representing Civil Engineering

Redacted for privacy

Head of the Department of Civil, Construction and Environmental Engineering

Redacted for privacy

Dean of the Graduate School

I understand that my thesis will become part of the permanent collection of Oregon State University libraries. My signature below authorizes release of my thesis to any reader upon request.

Redacted for privacy

Adrian Kidarsa, Author

ACKNOWLEDGEMENTS

The author wishes to express sincere gratitude to Professor Scott for his patience and excellent guidance throughout the course of the author's graduate school experience. A special appreciation to Professor Higgins who provided technical support, data gathering and interpretation efforts. The author is thankful to his coworkers, who had been very supportive in research efforts and education. Lastly, a very special thank you to the author's family for their never ending support.

CONTRIBUTION OF AUTHORS

This thesis is written through a collaboration of three authors. Professor Scott provided insightful theoretical knowledge, technical expertise, and data interpretation. He assisted in the design and writing of the chapters in the thesis. Professor Higgins contributed technical expertise, experimental data and interpretations of results.

TABLE OF CONTENTS

TABLE OF CONTENTS (Continued)

LIST OF FIGURES

LIST OF FIGURES (Continued)

LIST OF TABLES

General Introduction

Structures subjected to moving loads often require a periodic assessment of their capacity for comparison with demands imposed by the loads. An example assessment methodology is the rating of highway bridges for moving truck loads. Analysis for moving loads requires accurate computation of structural response quantities to determine the position or combination of loads that produce the highest demand at critical locations. Example of critical sections include flexural reinforcement cutoffs, changes in stirrup spacing in reinforced concrete members, section transitions in built-up steel members, etc.

Compared to classical structural analysis methods such as slope-deflection or moment-distribution, computerized structural analysis programs provide an efficient approach to moving load analysis. The programs allow repeated analysis of different load positions and complex load combinations to compute the maximum demand at specified locations in a structure. State of the art analysis programs are based on finite element methods, for which there are two fundamental mathematical formulations for the beam-column elements that simulate the response of structural members.

The most common element formulation is the displacement-based formulation, which follows the general finite-element approach of prescribing an approximate displacement field along the element. Due to weak equilibrium of moving loads, nodes must be placed at the critical sections along a member (mesh refinement) to determine the required response quantities. The internal forces at the critical locations correspond to element end forces of the discretized model. This approach ensures accuracy of the element response, but is not ideal since it requires additional nodes in the finite element model.

The second element formulation is the force-based formulation, which imposes strong equilibrium along the element. The equilibrium condition alleviates the need for mesh refinement to compute internal forces in a structural member subjected to moving loads. The internal forces are computed at the integration points of the element. Numerical integration error is the only error present in the formulation. By specifying the location of critical sections as the element integration points, the section forces can be determined accurately while keeping to a minimum the size of the model.

This thesis consists of two manuscripts. The first manuscript discusses the application of force-based element in the moving load analysis of prismatic structural members. The manuscript has two objectives. First, it demonstrates the advantages of using the force-based finite element in moving load analysis compared to displacement-based elements. Second, to overcome the constraints imposed by optimal Gauss-based quadrature, a low order numerical integration approach is developed in order to allow critical sections to be specified as integration points for the element.

The second manuscript explores moving load analysis of nonprismatic structural members using force-based elements. The first objective is to study the effects of using force-based elements in simulating the response to moving loads of members with varying cross-section properties. The second objective is to demonstrate the force-based element computations (using the low order integration approach developed in the first manuscript) in simulating test truck data recorded at an Oregon highway overpass with tapered bridge girders.

Analysis of Moving Loads Using Force-Based Finite Elements

Adrian Kidarsa, Michael H. Scott, Christopher C. Higgins

Journal of Structural Engineering
1801 Alexander Bell Drive
Reston, VA 20191
Submitted for review (ST24937)

Analysis of Moving Loads Using Force-Based Finite Elements

Adrian Kidarsa[1], Michael H. Scott[2], and Christopher C. Higgins[3]

CE Database: Finite elements, Influence lines, Moving loads, Numerical integration, Simulation models, Structural analysis

ABSTRACT

An analysis method for moving loads computes the internal demand history in a structural member at the integration points of force-based finite elements as opposed to the end forces of a refined displacement-based finite element mesh. The force-based formulation satisfies strong equilibrium of internal section forces with the element end forces and the moving load. This is in contrast with displacement-based finite element formulations that violate equilibrium between the section forces and the equivalent end forces computed for the moving load. A new approach to numerical quadrature in force-based elements allows the specification of integration point locations where the section demand history is critical while ensuring a sufficient level of integration accuracy over the element domain. Influence lines computed by numerical integration in force-based elements converge to the exact solution and accurate results are obtained for

[1] Graduate Research Assistant, Dept. of Civil Engineering, Oregon State University, Corvallis, OR 97331. e-mail: kidarsa@engr.orst.edu
[2] Assistant Professor, Dept. of Civil Engineering, Oregon State University, Corvallis, OR 97331 (corresponding author). e-mail: michael.scott@oregonstate.edu
[3] Associate Professor, Dept. of Civil Engineering, Oregon State University, Corvallis, OR 97331. e-mail: chris.higgins@oregonstate.edu

practical applications in structural engineering through the new low-order integration approach.

INTRODUCTION

Moving load analysis requires an accurate computation of structural response quantities in order to determine the position or combination of live loads that will produce the highest demand at critical locations in a structure. Examples of critical locations are flexural bar cutoffs or changes in stirrup spacing in reinforced concrete members and section transitions in built-up steel members. Influence lines show the variation of a particular response quantity (shear force, bending moment, etc.) at a location as a unit load moves across the structure. An influence line can then be used to evaluate the magnitude of the response quantity for more complex loading events. Influence lines are particularly useful for the analysis of vehicle loads on bridge structures, loads on crane runways, and live load patterns in multi-story frame structures.

Qualitative influence lines can be constructed using the Müller-Breslau principle described in structural analysis texts; however, it is often necessary to generate quantitative influence lines for structural design and assessment. Classical structural analysis methods, such as moment distribution and slope-deflection, become relatively time consuming when used to construct quantitative influence lines. Computerized structural analysis programs provide a more efficient alternative by allowing repeated analyses for several positions of a moving load. Such programs are based on the finite element method, for which there are two types of formulations for the beam-column elements used to simulate the response of structural members for each location of a moving load.

The first method is the displacement-based formulation, which follows the finite element approach of prescribing an approximate displacement field along the element (Hughes 1987, Cook *et al* 1989, Zienkiewicz and Taylor 2000). The displacement fields for standard beam-column finite element implementations, e.g., assumed linear axial displacement and cubic Hermitian transverse displacement fields, do not account for interior element loads, such as a point load that moves across the element domain. Consistent with the principle of virtual displacements, the computation of equivalent end forces for the finite element solution produces a weak equilibrium error between the element end forces, the moving load, and the internal section forces along the element. This error is mitigated by placing a node at each critical location along the member (h-refinement) and treating the internal forces of the member as the end forces of the elements in the refined mesh. The drawback to this approach is it decouples the internal member force computation from a constitutive relationship that accounts for the interaction of internal forces at the critical location.

The second approach to simulate beam-column response is the force-based formulation (Spacone *et al* 1996), which imposes strong equilibrium of internal section forces with the element end forces and loads applied on the element interior. This equilibrium condition alleviates the need for mesh refinement in order to compute the internal forces in a structural member subjected to a moving load. The internal forces are computed at the integration points of the finite element and only a numerical integration error is present in the analysis. The drawback to the force-based approach, however, is the integration point locations seldom coincide with critical locations along the structural member. As a result, it is difficult to compute the internal section forces at specified critical locations when using force-based elements to simulate the response of a structure to moving loads.

This paper has two main objectives: 1) to demonstrate the advantages of using force-based finite elements in the moving load analysis of structures; and 2) to develop an approach to numerical integration in force-based finite elements where critical section locations are specified as the element integration points. First, an overview of the force-based formulation is presented, along with a comparison of the internal equilibrium conditions that arise in the displacement- and force-based formulations due to a point load that moves along a simply-supported structural member. Optimal quadrature methods that have a high order of integration accuracy are summarized next, followed by the development of the new low-order integration approach that allows the location of each integration point to be specified along with the associated integration weights at a selected number of points. The remaining integration weights are computed in order to ensure numerical integration accuracy over the entire element domain. This paper concludes with example applications that demonstrate the numerical accuracy of the new integration approach in force-based elements is on par with that offered by optimal quadrature rules, but with the important advantage of computing the internal force history at critical locations along a structural member during a moving load analysis.

FORCE-BASED FINITE ELEMENT FORMULATION

The force-based beam elements considered in this paper are formulated in a two-dimensional basic system, free of rigid body displacement modes (Filippou and Fenves 2004). The simply-supported basic system is shown in Fig. 2.1, where the basic forces (axial force and end moments) are collected in the vector

$$\mathbf{q} = [q_1 \quad q_2 \quad q_3]^T \tag{1}$$

The corresponding element deformations are the change in length and the end rotations:

$$\mathbf{v} = [v_1 \quad v_2 \quad v_3]^T \tag{2}$$

The internal forces at any location, x, along the element are collected in the section force vector:

$$\mathbf{s}(x) = [P(x) \quad M(x) \quad V(x)]^T \tag{3}$$

where P is the section axial force, M is the section bending moment, and V is the section shear force (Fig. 2.1). The corresponding section deformations are collected in the vector:

$$\mathbf{e}(x) = [\varepsilon(x) \quad \kappa(x) \quad \gamma(x)]^T \tag{4}$$

where ε is the axial deformation, κ is the curvature, and γ is the shear deformation of the section, each of which is work-conjugate to the corresponding value in $\mathbf{s}(x)$. Equilibrium between section forces and the basic forces and applied element loads is expressed in strong form:

$$\mathbf{s}(x) = \mathbf{b}(x)\mathbf{q} + \mathbf{s}_p(x) \tag{5}$$

The matrix $\mathbf{b}(x)$ contains the force interpolation functions that represent the homogeneous solution to beam equilibrium (constant axial and shear forces with linearly varying bending moment):

$$\mathbf{b}(x) = \begin{bmatrix} 1 & 0 & 0 \\ 0 & x/L-1 & x/L \\ 0 & 1/L & 1/L \end{bmatrix} \tag{6}$$

The vector $\mathbf{s}_p(x)$ in Eq. (5) represents the particular solution to beam equilibrium for an interior element load applied in the basic system. Expressions for $\mathbf{s}_p(x)$ considering several types of element loading are found in structural analysis texts. For a transverse point load, F, located a distance x_0 along an element, this vector is

$$\mathbf{s}_p(x) = \begin{bmatrix} 0 \\ FL\xi_0(1-\xi_0)(1-(\xi_0-\xi)/\xi^*) \\ F\xi_0(1-\xi_0)/\xi^* \end{bmatrix} \tag{7}$$

where $\xi = x/L$ and $\xi_0 = x_0/L$, as shown in Fig. 2.2, and

$$\xi^* = \begin{cases} \xi_0 & \xi \le \xi_0 \\ \xi_0 - 1 & \xi > \xi_0 \end{cases} \tag{8}$$

For a transverse load that moves across the element, the section forces in Eq. (7) evolve as a function of the position variable ξ_0. An important advantage of the force-based formulation is the ability to account for section shear force directly in the element equilibrium relationship (Ranzo and Petrangeli 1998). For moving load analysis, the section shear force is computed from static equilibrium of the basic forces and the interior point load applied at a given location.

The section forces are related to the section deformations through a constitutive relationship. In this paper, linear-elastic section response is considered, where the section forces are expressed as a matrix-vector product of the section deformations:

$$\mathbf{s}(x) = \mathbf{k}_s(x)\mathbf{e}(x) \tag{9}$$

where $\mathbf{k}_s$ is the matrix of section stiffness coefficients derived from the material properties and dimensions of the cross-section. In the force-based formulation, it is necessary to express the section force-deformation relationship of Eq. (9) in compliance form:

$$\mathbf{e}(x) = \mathbf{f}_s(x)\mathbf{s}(x) \tag{10}$$

where $\mathbf{f}_s(x) = \mathbf{k}_s^{-1}(x)$ is the section flexibility matrix.

According to the principle of virtual forces, along with Eqs. (5) and (10), the element compatibility relationship in the force-based formulation is expressed in integral form:

$$\mathbf{v} = \left(\int_0^L \mathbf{b}^T(x)\mathbf{f}_s(x)\mathbf{b}(x)dx \right)\mathbf{q} + \int_0^L \mathbf{b}^T(x)\mathbf{f}_s(x)\mathbf{s}_p(x)dx \qquad (11)$$

It is assumed in this paper that Eq. (11) is evaluated by an N-point numerical integration rule as a summation of N discrete function evaluations at locations, x_1, ..., x_N, with associated integration weights, w_1, ..., w_N:

$$\mathbf{v} = \left(\sum_{i=1}^{N} \mathbf{b}^T(x_i)\mathbf{f}_s(x_i)\mathbf{b}(x_i)w_i \right)\mathbf{q} + \sum_{i=1}^{N} \mathbf{b}^T(x_i)\mathbf{f}_s(x_i)\mathbf{s}_p(x_i)w_i \qquad (12)$$

For a prismatic element, $\mathbf{f}_s(x)$ is constant along the length, and quadratic polynomials appear in the first term on the right-hand side of Eq. (12) from the squaring of the linear interpolation functions in $\mathbf{b}(x)$, thus it is possible to evaluate this term exactly with a quadrature rule that exactly integrates quadratic polynomials. The second term on the right-hand side of Eq. (12) contains a discontinuity in $\mathbf{s}_p(x)$ when a transverse point load is applied on the element interior, which is evident from the jump in the shear diagram of Fig. 2.2. Consistent with numerical analysis theory, an error will appear from evaluating this term by numerical integration because the stated accuracy of any quadrature method is based on the assumption of smoothness, or continuity,of the integrand and its derivatives (Stoer and Bulirsch 1993).

With the overview of the force-based formulation complete, the difference between the displacement- and force-based formulations is illustrated in the moving load analysis of the simply-supported beam shown in Fig. 2.2. The analysis is performed with a single displacement-based element (cubic Hermitian polynomials for the transverse displacement field), and then the analysis is repeated using a single force-based element. The governing equations in each element formulation are evaluated by three-point Gauss-Lobatto quadrature in order to compute an influence line for the midspan bending moment. As seen in Fig. 2.3, there is a significant error in the influence line computed with one displacement-based element since the internal bending moment is constrained to the equivalent end moments computed from the transverse displacement field. On the other hand, the analysis with one force-based element captures the exact solution. There is no numerical integration error in the force-based solution because the structure is statically determinate, i.e., no compatibility equations have to be satisfied by the analysis. The exact solution for the midspan moment influence line in the displacement-based formulation can be obtained by subdividing the span into two elements with an additional node at midspan. The midspan moment is then equal to the end moments of the adjacent elements; however, this approach is less than ideal because it requires refinement of the finite element mesh and it decouples the internal force computation from a constitutive model that accounts for the interaction of section forces at the element integration points.

OPTIMAL ELEMENT INTEGRATION METHODS

This section contains an overview of two optimal numerical integration methods that integrate the highest order polynomial possible under the given constraints on the integration point locations and weights. First is Gauss-Lobatto quadrature, which is commonly used in the implementation of force-based finite elements. This is followed by the method of undetermined coefficients, of which Newton-Cotes quadrature is a special case.

Gauss-Lobatto Quadrature

Gauss-Lobatto quadrature (Abramowitz and Stegun 1972) is the standard approach to evaluate the element integral (Eq. (12)) in the force-based formulation because it places sample points at the element ends, where bending moments are largest in the absence of interior element loads. This quadrature method exactly integrates polynomials up to order 2N-3, i.e., from x^0 to x^{2N-3}, where N is the number of sample points. In addition to its high order of accuracy, Gauss-Lobatto quadrature is numerically stable since all integration weights are positive for any selection of N. The primary disadvantage to this approach is the locations and weights of the sample points are determined from optimality conditions for the integration of high-order polynomials that are rarely encountered in practical structural engineering applications. Accordingly, neither the locations nor the weights of the sample points (excluding those at the element ends) have any correlation to the physical characteristics of a structural system, e.g., the location of bar cut-offs, changes in stirrup spacing, or observed plastic hinge lengths (Scott and Fenves 2006). Furthermore, the high order of integration accuracy for this quadrature method in the force-based formulation is compromised because discontinuities appear in the integrand of Eq. (12) in the presence of interior point loads.

Method of Undetermined Coefficients

To alleviate the optimality constraints imposed by the Gauss-Lobatto quadrature method, it is possible to specify the location of each sample point and construct a quadrature method of a lower order of integration accuracy. This approach treats the N sample point locations, $x_1,\ldots,x_N$, as known values while the associated weights, $w_1,\ldots,w_N$, are computed in order to ensure exact integration of polynomials up to order N-1. The integration weights are found by the solution for the undetermined coefficients in the Vandermonde system (Golub and Van Loan 1996):

$$\begin{bmatrix} 1 & 1 & \cdots & 1 \\ x_1 & x_2 & \cdots & x_N \\ \vdots & \vdots & \ddots & \vdots \\ x_1^{N-1} & x_2^{N-1} & \cdots & x_N^{N-1} \end{bmatrix} \cdot \begin{bmatrix} w_1 \\ w_2 \\ \vdots \\ w_N \end{bmatrix} = \begin{bmatrix} b-a \\ (b^2-a^2)/2 \\ \vdots \\ (b^N-a^N)/N \end{bmatrix} \tag{13}$$

where [a, b] is the interval of integration. Although this approach to constructing a quadrature rule permits complete control over the location of sample points in a force-based element, there is no control over the resulting integration weights. In fact, this approach is generally unstable because negative integration weights can appear for any $N \geq 2$, i.e., the sum of the absolute values of the integration weights is greater than the length of the integration domain. Negative integration weights can lead to a non-unique solution where the computed response can change significantly as a function of the number and location of sample points. It is noted that the solution of the Vandermonde system in Eq. (13) for equally spaced sample point locations generates the Newton-Cotes quadrature method (Abramowitz and Stegun 1972), which is stable for any $N < 9$.

LOW-ORDER APPROACH TO UNDETERMINED COEFFICIENTS

As discussed in the previous section, neither Gauss-Lobatto quadrature nor the method of undetermined coefficients permits complete control over the location and weight of each sample point. Furthermore, negative integration weights can appear via the method of undetermined coefficients by forcing the resulting quadrature rule to represent polynomials up to order N-1, thereby leading to numerical instability and non-uniqueness of the computed solution.

In this section, an alternative approach is taken to the method of undetermined coefficients to construct an N-point quadrature rule with specified point locations. This approach is based on the following observations:

1. There will be a numerical integration error for any quadrature method that is used to evaluate the force-based element compatibility relationship

when a transverse point load is applied on the element interior and causes a discontinuity of the integrand in Eq. (12).

2. For the common case of a prismatic element without interior loads ($\mathbf{s}_p(x) = \mathbf{0}$), the integration of quadratic polynomials is sufficient to represent the product of a linear curvature distribution with the linear bending moment interpolation functions in Eq. (12).

From these observations, it is seen that for an N-point quadrature rule with specified locations, only three integration weights need to be treated as unknown in order to integrate up to quadratic polynomials, i.e., x^0, x^1, and x^2, which are necessary to represent a linear curvature distribution along an element. As a result, the remaining N-3 weights can be specified in addition to the N locations while maintaining a sufficient level of numerical accuracy for elements without interior point loads.

To formalize this procedure of constructing an N-point quadrature rule with specified locations and partially specified weights, the integration points are divided into two groups, those constrained to have a specified weight and those where the weight is treated as unknown. The number of integration points where the corresponding weight is specified is N_c, while $N_f = N-N_c$ is the number of integration points where the associated weight is unknown. Accordingly, the integration point locations are denoted x_f and x_c, while the weights are w_f and w_c. A Vandermonde system on the order of N_f can then be solved to obtain the unknown weights, which will ensure accurate integration of polynomials up to the order of N_f - 1. Consequently, Eq. (13) is modified by moving to the right-hand side the contributions of the N_c integration points for which both the location and weight are specified:

$$\begin{bmatrix} 1 & 1 & \cdots & 1 \\ x_{f1} & x_{f2} & \cdots & x_{fN_f} \\ \vdots & \vdots & \ddots & \vdots \\ x_{f1}^{N_f-1} & x_{f2}^{N_f-1} & \cdots & x_{fN_f}^{N_f-1} \end{bmatrix} \cdot \begin{bmatrix} w_{f1} \\ w_{f2} \\ \vdots \\ w_{fN_f} \end{bmatrix} = \begin{bmatrix} (b-a) - \sum_{j=1}^{N_c} w_{cj} \\ (b^2 - a^2)/2 - \sum_{j=1}^{N_c} x_{cj} w_{cj} \\ \vdots \\ (b^{N_f} - a^{N_f})/N_f - \sum_{j=1}^{N_c} x_{cj}^{N_f-1} w_{cj} \end{bmatrix} \tag{14}$$

To ensure the integration rule can represent a linear curvature distribution, which occurs in the analysis of prismatic structural members without interior loads, $N_f \geq 3$ is required. Although this approach does not guarantee that all integration weights computed via Eq. (14) will be positive, it makes the resulting quadrature rule physically significant by allowing the integration weights to be specified at selected locations and removes the constraints of integrating high-order polynomials that are rarely encountered in structural engineering applications. Thus, this numerical integration approach is suited to represent nonlinear material response over prescribed lengths in a structural member, e.g., in plastic hinge zones of beam-column members and in shear critical D-regions adjacent to continuous beam supports.

NUMERICAL EXAMPLES

The Gauss-Lobatto quadrature rule and the low-order approach to the method of undetermined coefficients presented in this paper have been implemented in the OpenSees finite element software framework (McKenna *et al* 2000). The convergence behavior of each approach to numerical integration in the force-based formulation is investigated for computing influence lines in the first example. Then, applications to the moving load analysis of a bridge structure are explored in the second example.

Convergence of Influence Lines for Each Quadrature Method

In this example, moment and shear influence lines computed by the integration methods presented in this paper are compared to the exact solution for the bending moment and shear forces developed at sections A and B in the two-span structure shown in Fig. 2.4. Section A is at the middle of span one, a location of high moment and low shear; whereas section B is located at the right end of span one, just to the left of the continuous support, at a negative moment location with high shear. The structure has a prismatic cross-section and linear-elastic material properties for flexural and shear deformations at each section. Poisson's ratio is assumed to be 0.3 and the radius of gyration for the cross-section is 0.394m. Each span length is L = 15 m.

The convergence of the computed influence lines is demonstrated using a single force-based finite element per span with N = 3, 5, 7, and 9 integration points in each quadrature method. An odd number of integration points in the Gauss-Lobatto and Newton-Cotes methods will ensure that internal forces will be sampled at sections A and B of the structure. For the quadrature approaches based on undetermined coefficients, integration points are placed at the middle and at the ends of each element with successive integration points placed on the interior of the domain for N > 3. For the low-order approach, the weights at the middle three integration points are treated as undetermined coefficients, while the weights at the remaining N-3 integration points are set equal to 0.05L. These integration point locations are shown in Fig. 2.5, and the associated integration weights computed by Eqs. (13) and (14) for each approach are listed in Table 2.1.

The results of the moving load analysis using the Gauss-Lobatto and the low-order undetermined coefficients integration methods with N = 5 are shown in Fig. 2.6 as influence lines for the internal moment and shear at sections A and B of the two-span structure. As seen in Fig. 2.6(a), the computed solution matches the exact solution for the moment and shear influence lines at section A, where flexural response dominates. At section B, with negative moment and high shear, there is a noticeable error in the computed solution for the moment influence line shown in Fig. 2.6(b). This error is significant in both the Gauss-Lobatto and the low-order integration approaches, and it arises from the change in sign of the section shear force interpolated from the moving load as the load moves across each integration point. As seen in the shear diagram of Fig. 2.2, when the load is just to the left of a particular section, the section shear force is positive. Then the load moves just to the right of the section and the shear force suddenly changes to a negative value. These errors are more significant at the shear critical section B than at section A because the effect of shear deformation on the element compatibility relationship is negligible at midspan. It is noted that numerical errors occur at the critical sections in the first span even as the load moves across the second span because the numerical error of the element compatibility relationship in the second span will propagate throughout the structure.

To summarize the convergence behavior of each integration approach (Gauss-Lobatto, Newton-Cotes, undetermined coefficients, and low-order undetermined coefficients) as the number of integration points increases, the error between the computed and exact solution is determined according to the definition

$$E(i) = \left| \frac{R(i) - R_{exact}(i)}{R_{\max}} \right| \cdot 100 \tag{15}$$

where i indicates a location ordinate as the load moves across the structure, R is the response ordinate, and R_{max} is the maximum response over all location ordinates in the exact solution. Scaling the absolute error by R_{max} rather than $R_{exact}(i)$ avoids spuriously large relative errors when the exact solution for the response ordinate is close to zero. The maximum percent error over all values of the location ordinate is shown in the bar charts in Figs. 2.7 and 2.8 for sections A and B, respectively. Each integration method gives identical results with N = 3, for which the well-known Simpson's rule is recovered in all cases. Gauss-Lobatto quadrature has the highest rate of convergence for increasing N, while the low-order approach converges at the slowest rate because the integration accuracy stays constant with increasing N. Newton-Cotes quadrature shows a reduction in the percent error up to N = 9, in which case a negative integration weight appears, causing the error to increase. There is a lack of convergence of the computed result to the exact solution with the method of undetermined coefficients for $N \geq 5$ due to the appearance of negative integration weights from the solution to Eq. (13) for the locations specified in Fig. 2.5.

Application to Bridge Analysis

The application of the low-order undetermined coefficients integration method in the force-based element formulation to computing the moment-shear demand history at critical sections in a structure is presented in this example for the moving load analysis of a conventionally reinforced concrete deck girder bridge. The structure is the McKenzie River Bridge, located on Interstate-5 just north of Eugene, OR, and shown schematically in Fig. 2.9. Each span is 15.25 m long and the girder is 1.22 m deep and 0.33 m wide. Prismatic, linear-elastic response is assumed along each span using the elastic properties of concrete and the girder cross-section dimensions. A three-axle AASHTO HS-20 design truck (AASHTO 1998) moves across the bridge.

A single force-based element is used to compute the response of each span, and the integration points for each element correspond to the seven span locations identified as critical for rating (Higgins *et al* 2005). These critical locations, shown in Fig. 2.9, represent changes in stirrup spacing, flexural reinforcing steel cut-off locations, and locations of diagonal cracks from inspection data. To construct a quadrature method that uses these locations in the low-order approach to numerical integration, an integration weight of 1.83 m is assigned to sections 1 and 7, while a weight of 1.22 m (equal to the depth of the bridge girder) is assigned to sections 2 and 6. The remaining integration weights at sections 3, 4, and 5 are determined by the solution of Eq. (14) to be approximately 2.74, 3.67, and 2.74 m, respectively.

The internal moment and shear demand history at each critical location due to the moving load pattern is computed using one force-based beam element in each span with the locations and weights of the integration points described above. The analysis results are shown in Fig. 2.10 for the moment and shear at the middle of span one and at the farthest right location (section 7) in span two, 29.3 m from the left abutment. The computed moment and shear demand histories are very close to the exact solution, as shown in Fig. 2.10. The errors for the moment and shear at the middle of span one are 1.63% and 1.18%, respectively. Similarly, the errors for the moment and shear at 29.3 m from the left abutment are 4.93% and 0.785%, respectively. Considering the large amount of uncertainty in estimating structural capacity from design drawings, material properties, and field inspection data, this small difference between the computed and exact solution indicates that specifying critical sections as integration points within a force-based element using low-order integration is an accurate and reliable approach to computing the internal demands of a structure subjected to moving loads.

CONCLUSIONS

The advantages of using force-based finite elements in the moving load analysis of structures have been demonstrated. Since the force-based formulation imposes strong equilibrium between the section forces and the end moments and interior element loads, only a single force-based finite element is required to simulate the response of a structural member to moving loads. Further discretization of the finite element model is not necessary, even as additional critical locations are included in the analysis. A new numerical integration approach was presented that allows the specification of critical locations in a structural member as the integration points of a force-based element. This integration approach maintains a low order of integration accuracy that is sufficient for practical applications in structural engineering. Accurate results for the moment and shear demand history at specified locations in a structure were obtained using force-based elements in conjunction with the new integration approach. Although the numerical examples focused on linear-elastic structural response, further applications of this integration approach include the representation, using a single force-based finite element, of the spread of plasticity across prescribed plastic hinge lengths and the smearing of moment-shear interaction over D-regions at continuous structural supports.

ACKNOWLEDGEMENT

This work was supported by the Oregon Department of Transportation under grant number MBMSFY04-041 awarded to Oregon State University. Their support is gratefully appreciated.

Notation

The following symbols are used in this paper:

$\mathbf{b}$ = section force interpolation matrix;

$\mathbf{e}$ = section deformation vector;

$\mathbf{f}_s$ = section flexibility matrix;

$\mathbf{k}_s$ = section stiffness matrix;

N = number of element integration points;

$\mathbf{q}$ = element basic force vector;

$\mathbf{s}$ = section force vector;

$\mathbf{s}_p$ = section force vector due to interior element loads;

$\mathbf{v}$ = element deformation vector;

w = integration point weight; and

x = integration point location.

References

AASHTO (1998). *LRFD bridge design specifications*, 2nd ed., American Association of State Highway and Transportation Officials, Washington, D.C.

Abramowitz, M. and Stegun, I. A. (1972). "Handbook of Mathematical Functions with Formulas, Graphs, and Mathematical Tables, 9th printing." Dover, New York, NY.

Cook, R.D., Malkus, D.S., and Plesha, M.E. (1989). *Concepts and applications of finite element analysis*, 3rd ed., John Wiley and Sons, New York, NY.

Filippou, F.C. and Fenves, G.L. (2004). "Methods of analysis for earthquake-resistant structures." *Earthquake engineering: From engineering seismology to performance-based engineering*. Y. Bozorgnia and V. V. Bertero, etd., Chap. 6, CRC, Boca Raton, FL.

Golub, G.H. and Van Loan C.F. (1996). *Matrix computations*, 3rd ed, The Johns Hopkins University Press, Baltimore, MD.

Higgins, C., Daniels, T.K., Rosowsky, D.V., Miller, T.H., and Yim, S.C. (2005). "Reliability based assessment of conventionally reinforced concrete bridges for shear." Journal of the Transportation Research Board, Approved for publication 2005.

Hughes, T.J.R. (1987). *The finite element method*, Prentice-Hall, Englewood Cliffs, NJ.

McKenna, F., Fenves, G.L, Scott, M.H., and Jeremić, B. (2000). "Open system for earthquake engineering simulation." <http://opensees.berkeley.edu>.

Neuenhofer, A., and Filippou, F.C. (1997). "Evaluation of nonlinear frame finite-element models." Journal of Structural Engineering, 123(7), 958 – 966.

Ranzo, G., and Petrangeli, M. (1998). "A fibre finite beam element with section shear modelling for seismic analysis of RC structures." Journal of Earthquake Engineering, 2(3), 443-473.

Scott, M.H., and Fenves, G.L. (2006) "Plastic hinge integration methods for force-based beam-column elements," Journal of Structural Engineering, 132(2).

Spacone, E., Ciampi, V., and Filippou, F.C. (1996). "Mixed formulation of nonlinear beam finite element." Computers and Structures, 58, 71-83.

Stoer, J., and Bulirsch, R. (1993). *Introduction to numerical analysis*, 2nd ed., Springer-Verlag, New York, NY.

Zienkiewicz, O.C. and Taylor, R.L. (2000). *The finite element method: The basis*, 5th ed., Vol. 1, Butterworth, Stoneham, MA.

Table 2.1. Integration weights computed by undetermined coefficients and the low-order approach to undetermined coefficients in order to investigate the convergence behavior of each quadrature method.

			Undetermined Coefficients	**Low-order**
	i	x_i/L, 1.0-x_{N-i+1}/L	w_i, w_{N-i+1} (/ L)	w_i, w_{N-i+1} (/ L)
N = 3	1	0.0	0.1667	0.1667
	2	0.5	0.6667	0.6667
		$\sum\lvert w_i\rvert$/L	**1.0**	**1.0**
N = 5	1	0.0	-0.07357	0.05
	2	0.075	0.3325	0.1615
	3	0.5	0.4821	0.5770
		$\sum\lvert w_i\rvert$/L	**1.294**	**1.0**
N = 7	1	0.0	0.08781	0.05
	2	0.075	-0.2783	0.05
	3	0.125	0.4977	0.1432
	4	0.5	0.3857	0.5136
		$\sum\lvert w_i\rvert$/L	**2.113**	**1.0**
N = 9	1	0.0	-0.001350	0.05
	2	0.075	0.3714	0.05
	3	0.125	-0.6366	0.05
	4	0.175	0.6101	0.1241
	5	0.5	0.3219	0.4519
		$\sum\lvert w_i\rvert$/L	**3.561**	**1.0**

List of Figures

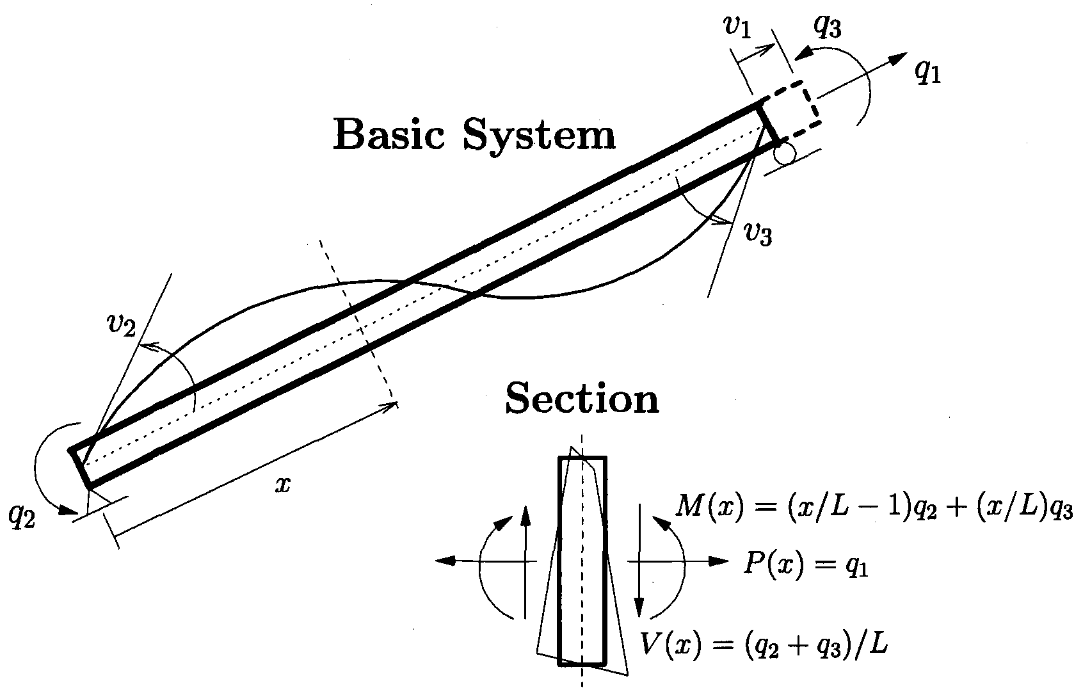

Figure 2.1. Simply-supported basic system and section forces for two-dimensional beam-column elements.

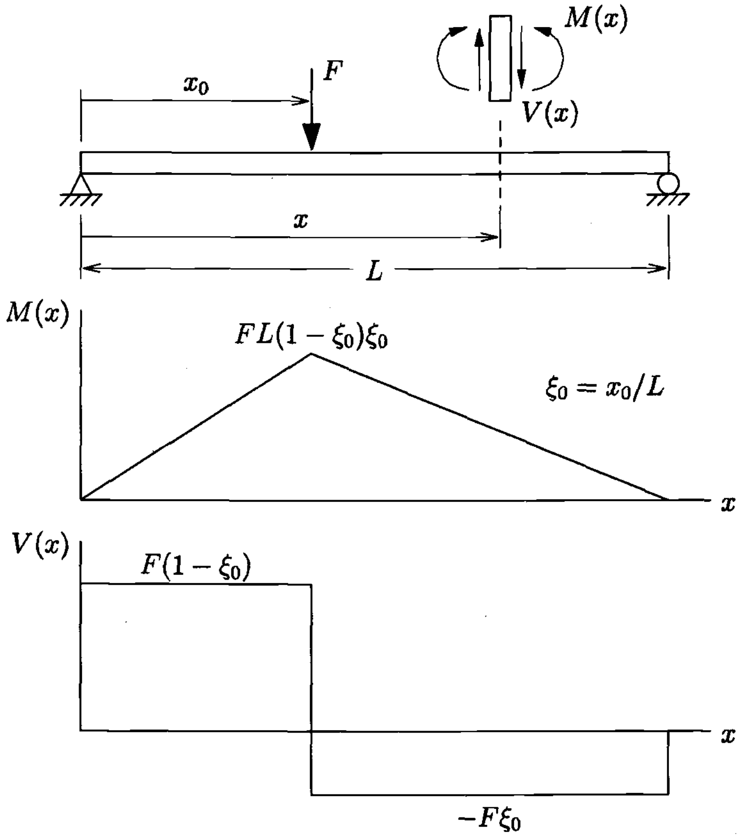

Figure 2.2. Bending moment and shear force developed in the simply-supported basic system for a transverse point load.

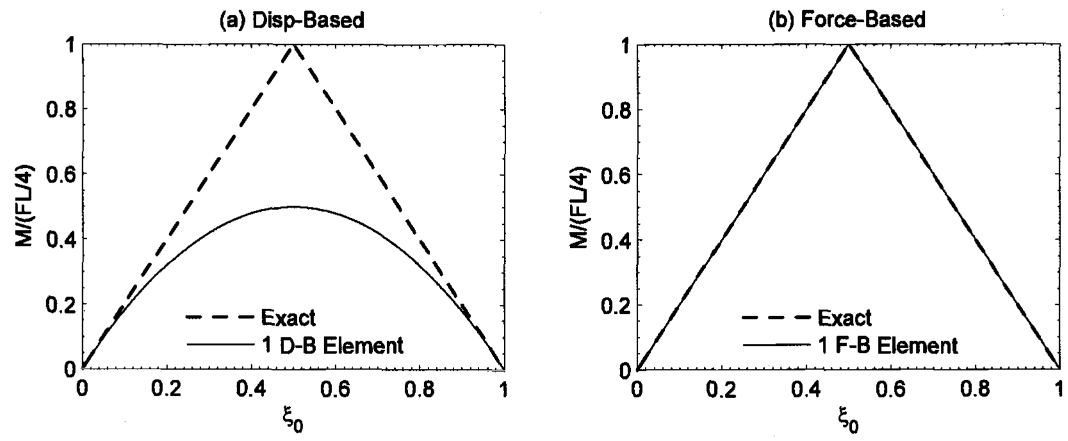

Figure 2.3. Comparison of the computed and exact solutions to the influence line for the midspan bending moment of a simply-supported beam using: (a) a single displacement-based element; and (b) a single force-based element.

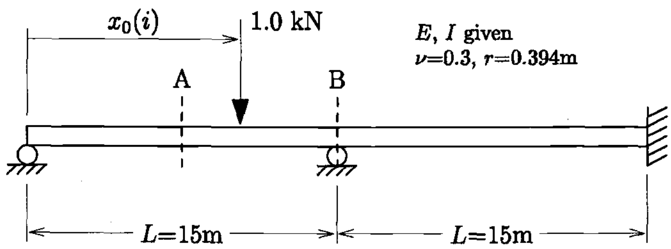

Figure 2.4. Two-span structure with a single force-based element along each span and internal forces computed at section A (middle of span one) and section B (end of span one) for a moving unit load.

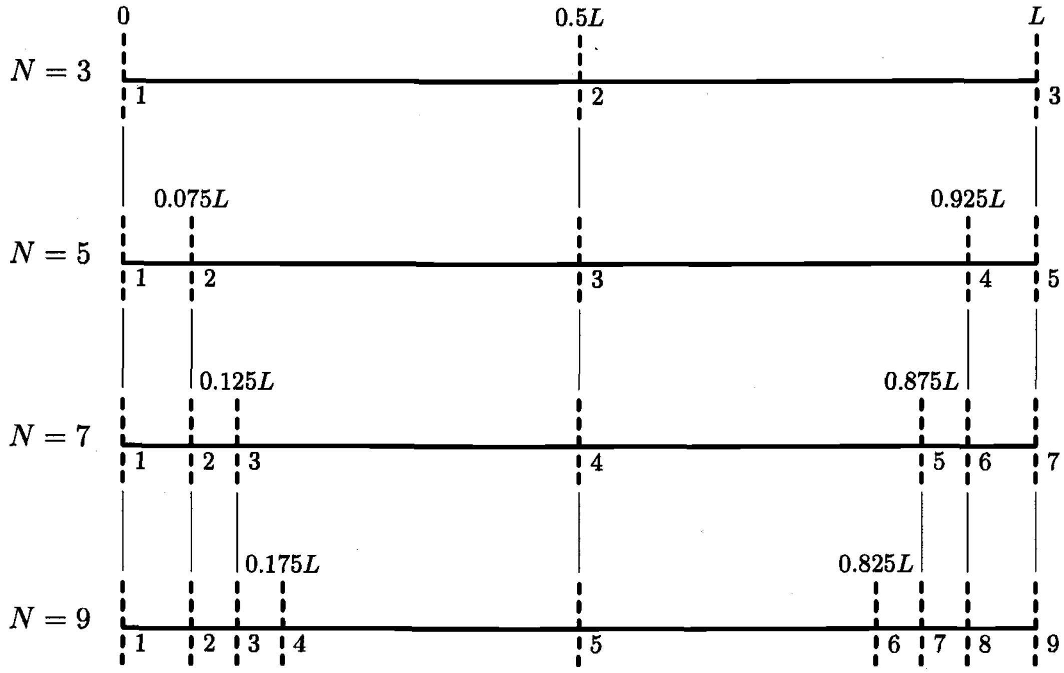

Figure 2.5. Integration point locations used in the undetermined coefficients and low-order undetermined coefficients approaches to demonstrate the convergence behavior of the moment and shear influence lines computed using a single force-based element in each span of the two-span structure in Fig. 2.4.

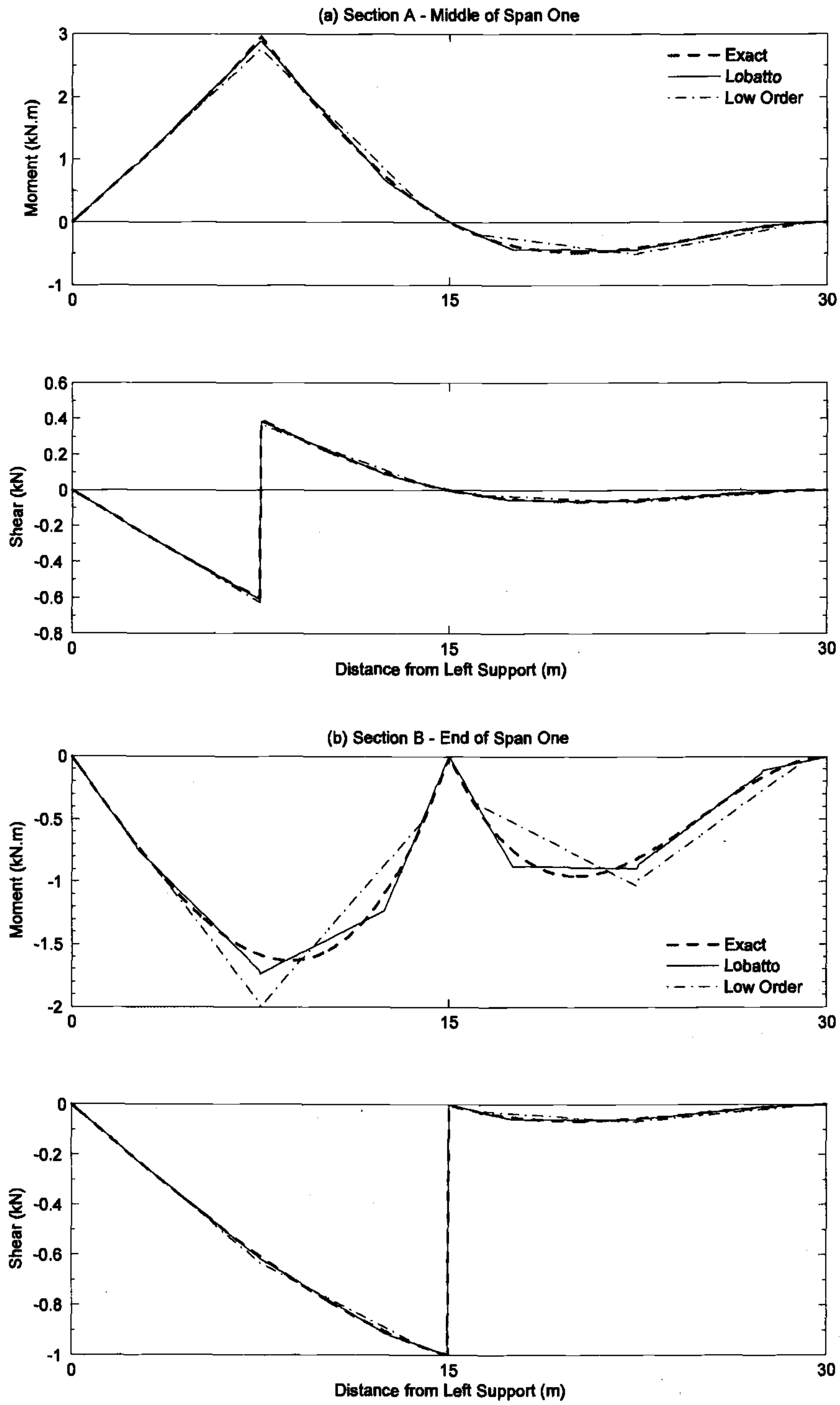

Figure 2.6. Moment and shear influence lines for the two-span structure of Fig. 2.4 computed with the five point (N=5) Gauss-Lobatto and low-order undetermined coefficients approaches: (a) middle of span 1; (b) right end of span 1.

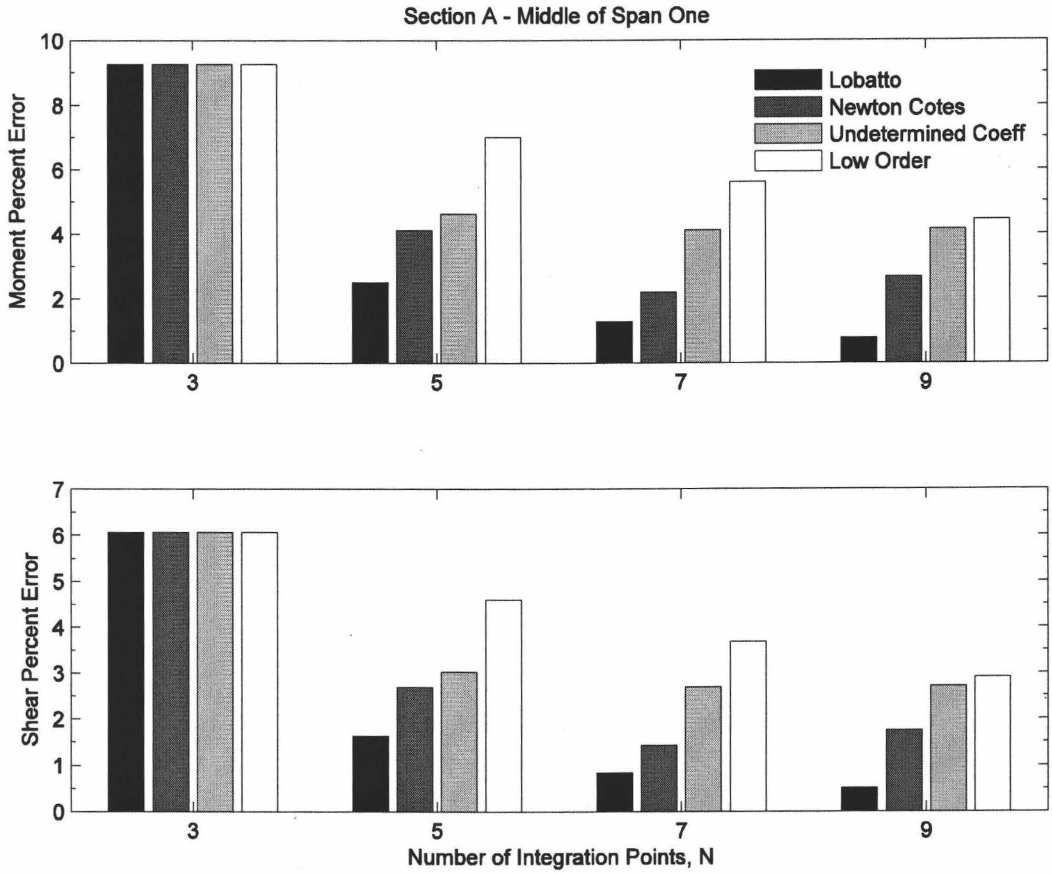

Figure 2.7. Percent errors for the internal moment and shear computed at section A of the two-span structure in Fig. 4 for each numerical integration approach with an increasing number of integration points.

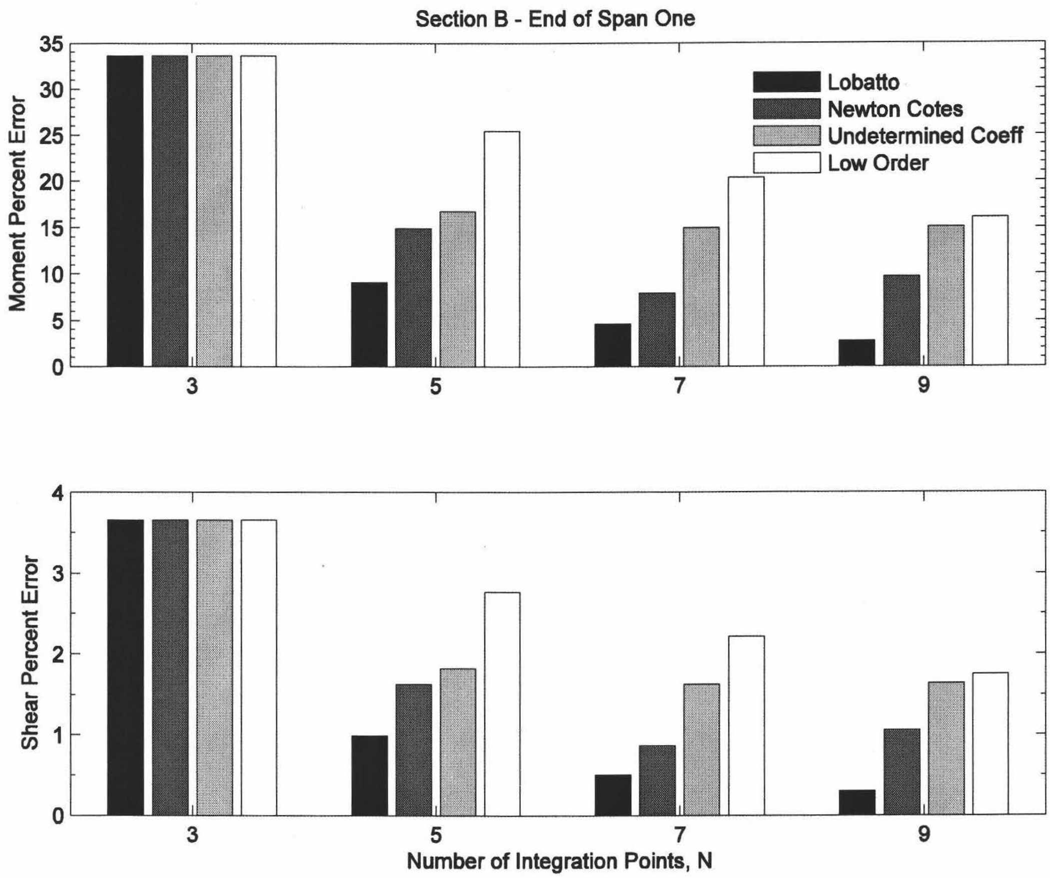

Figure 2.8. Percent errors for the internal moment and shear computed at section B of the two-span structure in Fig. 2.4 for each numerical integration approach with an increasing number of integration points.

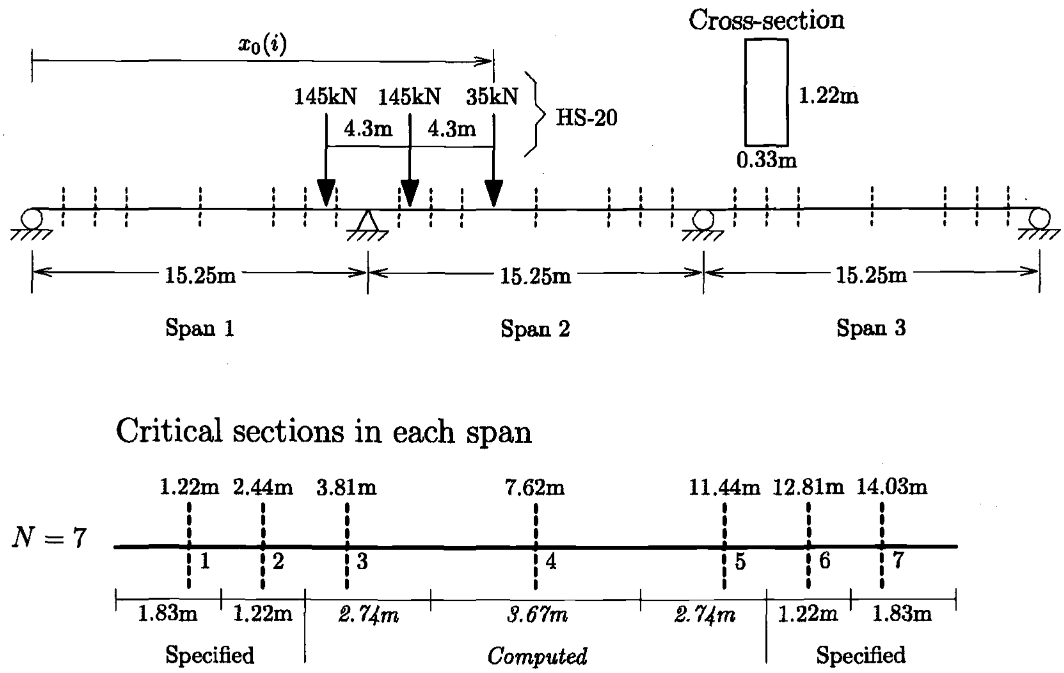

Figure 2.9. Model of the McKenzie River Bridge with seven section locations identified along each span as critical for rating.

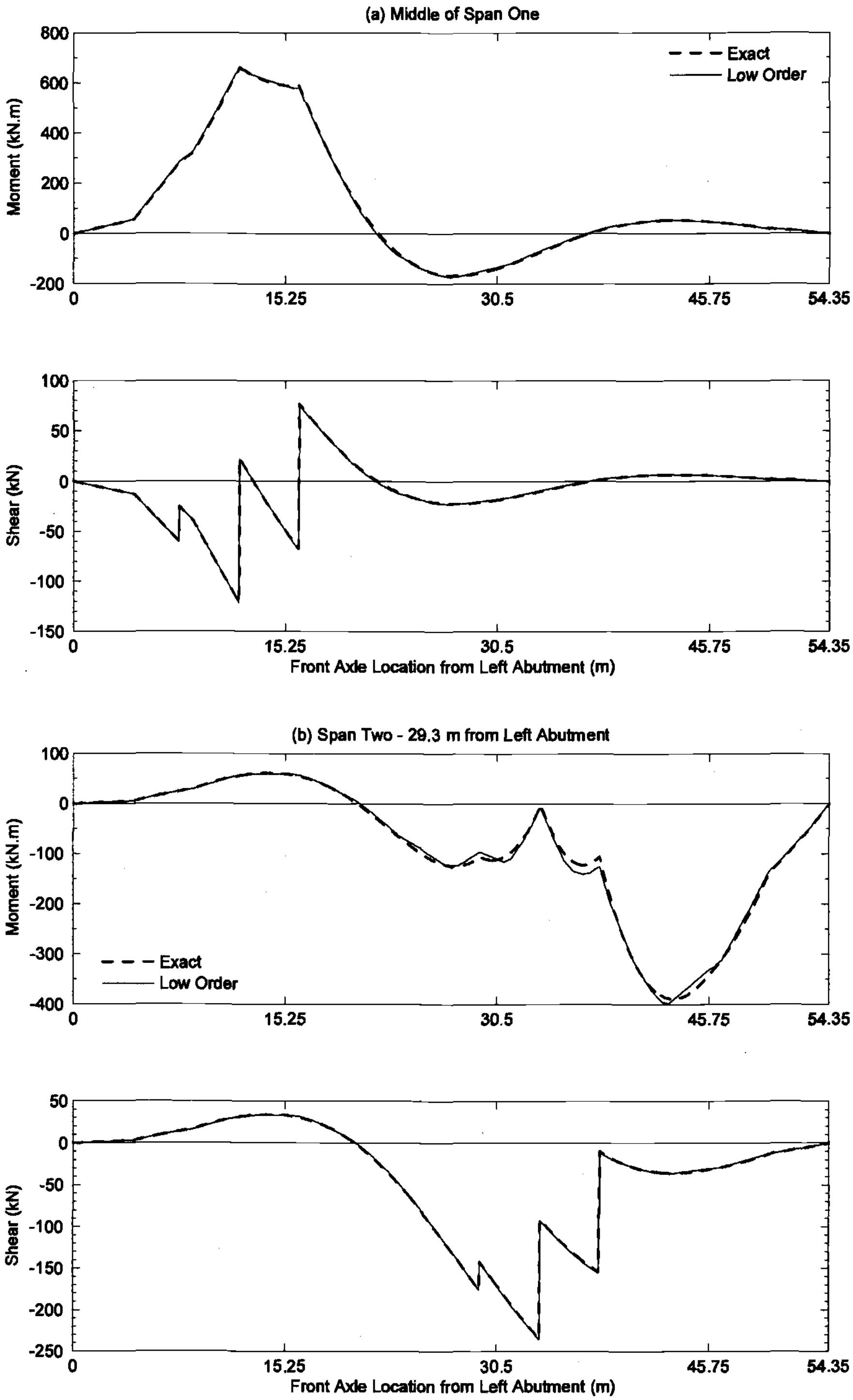

Figure 2.10. Comparison between the computed and exact solution for the moment and shear demand histories at: (a) middle of span 1; and (b) span 2 at 29.3 m from the left abutment of the McKenzie River Bridge.

Moving Load Analysis of Nonprismatic Bridge Girders Using Force-Based Finite Elements

Adrian Kidarsa, Michael H. Scott, Christopher C. Higgins

Journal of Bridge Engineering
1801 Alexander Bell Drive
Reston, VA 20191
To be published

Moving Load Analysis of Nonprismatic Bridge Girders Using Force-Based Finite Elements

Adrian Kidarsa[1], Michael H. Scott[2], Christopher C. Higgins[3]

CE Database: Structural analysis, Finite elements, Force-based, Moving loads, Numerical integration, Simulation model

ABSTRACT

The force-based finite element presents a method to analyze moving loads on nonprismatic structural members, which computes section demand histories at the integration points of the element, as opposed to obtaining section demands from the nodal forces of a refined displacement-based finite element. The force-based formulation satisfies strong equilibrium in the formulation such that only numerical integration errors appear in the computed results. Errors in the computed results can be mitigated by increasing the number of integration points. In contrast, the displacement-based element satisfies weak equilibrium between the element forces and the moving load(s). Discretization of element is necessary to reduce errors in the computed results. Using the Low-Order Undetermined Coefficients approach, sections of interest along the nonprismatic member can be

[1] Graduate Research Assistant, Dept. of Civil Engineering, Oregon State University, Corvallis, OR 97331. e-mail: kidarsa@engr.orst.edu
[2] Assistant Professor, Dept. of Civil Engineering, Oregon State University, Corvallis, OR 97331 (corresponding author). e-mail: michael.scott@oregonstate.edu
[3] Associate Professor, Dept. of Civil Engineering, Oregon State University, Corvallis, OR 97331. e-mail: chris.higgins@oregonstate.edu

specified as integration points on the force-based element. Influence lines computed by numerical integration in the force-based element converge to the exact solution, and accurate results are obtained for practical applications in bridge engineering using the Low-Order integration approach.

INTRODUCTION

Prismatic beams with various cross sections (rectangular, box, I-shape, etc.) have been used extensively in civil engineering structures. For economical or aesthetic reasons, nonprismatic beams are often utilized in structural applications. Examples of nonprismatic beams in structural design appear frequently in bridge design, where haunching of the girder cross section over the supports is very common. Tapering of reinforced concrete girders over continuous supports is also common. Other examples of nonprismatic beams in structural applications can be observed in large-span portal frame construction and light-frame steel structures. Structures with nonprismatic members can achieve a better distribution of strength and weight compared to structures with prismatic members.

There are many methods to analyze nonprismatic beam elements. The simplest approach utilizes the PCA handbook of frame constants for nonprismatic members, which provides design tables for nonprismatic beam elements with various cross sections. The handbook has been used in structural design practice for more than 35 years. El-Mezaini *et al* (1991) showed the PCA handbook of frame constants include significant errors, especially for deep haunches.

The most common approach utilizes finite element methods, which subdivides the nonprismatic beam into an equivalent number of prismatic elements. Results of the finite element approach converge to the exact solution with sufficient discretization of the model. The method can be time consuming and tedious with respect to data preparation. Typically finite element algorithms use the displacement based formulation, which cannot accommodate moving loads easily (Kidarsa *et al* 2006). Therefore, the finite element approach may not be convenient method for moving load analysis.

Just (1977) and Baker (1996) provide formulations of the exact stiffness matrix for nonprismatic beam elements. The formulations also provide methods to calculate equivalent nodal loads. The formulation allows one beam element to represent a non-prismatic beam. Discretization of the beam element model is not required. Furthermore, Brown (1983) derived a formulation of approximate bending stiffness matrix. Utilizing a cubic polynomial to obtain an approximate stiffness matrix, Brown provides results similar to Just (1977). Both formulations are derived for displacement-based elements, which may not provide accurate solutions in moving load analysis. The implementation of each formulation into a computer algorithm can be cumbersome.

Another approach to analyze nonprismatic beam elements utilizes the force-based finite element. Kidarsa *et al* (2006) shows the force-based formulation can provide a more convenient procedure in moving load analysis with respect to prismatic beam elements. With minor modifications, the force-based elements can provide a sufficient approximation in moving load analysis with respect to nonprismatic beam elements. It is more advantageous to use force-based finite elements in moving load analysis compared to the conventional displacement-based approach, when analyzing structures with nonprismatic members. The procedure can be easily implemented into a computer algorithm. In addition, application of the Low Order integration rule can be accommodated in the moving load analysis.

This paper presents the advantages of using force-based finite elements to model nonprismatic beam elements in moving load analysis. The paper begins with providing the necessary derivations for a nonprismatic force-based element. Statically determinate and statically indeterminate examples are presented to show the capability of the force-based formulation to provide excellent approximate solutions. An application to bridge analysis is presented to demonstrate the potential of the force-based formulation in moving load analysis. A comparison with experimental data is provided to validate the computed result from the force-based element.

FORCE – BASED ELEMENT FORMULATION

The force-based beam models considered in this paper are formulated in a basic system, free of rigid body displacement modes (Filippou and Fenves 2004). Although several basic systems are possible, the simply-supported system is chosen for derivation and implementation since its physical representation corresponds to the classical slope-deflection equations. Without loss of generality, axial forces are neglected and two-dimensional beam models are considered. The simply-supported basic system is shown in Fig. 3.1, where the basic forces are the end moments, q_2 and q_3, collected in the vector $\mathbf{q}$. The vector $\mathbf{v}$ collects the corresponding element deformations, v_2 and v_3, the nodal rotations relative to the rigid body rotation of the element chord. At any location x along the element length there are the vectors $\mathbf{s}(x)$ of internal section forces and $\mathbf{e}(x)$ of corresponding section deformations. The internal moment and shear force-deformation relationships are assumed to be linear-elastic:

$$\mathbf{e}(x) = \mathbf{f}_s(x)\,\mathbf{s}(x) \qquad (1)$$

where the section flexibility matrix, $\mathbf{f}_s(x)$, describes the variation of section properties (elastic modulus, area, moments of area) for a non-prismatic structural member.

In the numerical implementation of force-based beam elements (Spacone *et al* 1996, Neuenhofer and Filippou 1997), equilibrium between basic and section forces is satisfied in strong form at any given (pseudo-) time step during the analysis:

$$\mathbf{s}(x,t) = \mathbf{b}(x)\,\mathbf{q}(t) + \mathbf{s}_{\mathrm{p}}(x,t) \tag{2}$$

where $\mathbf{b}(x)$ contains force interpolation functions that represent the homogeneous solution to beam equilibrium, in which case the internal shear force is constant and the internal bending moment varies linearly along the element:

$$\mathbf{b}(x) = \begin{bmatrix} \dfrac{x}{L}-1 & \dfrac{x}{L} \\ \dfrac{1}{L} & \dfrac{1}{L} \end{bmatrix} \tag{3}$$

The vector $\mathbf{s}_{\mathrm{p}}$ in Eq. (2) represents the particular solution to equilibrium for time-varying loads applied on the beam interior. For the case of a transverse load, F, that moves a distance $x_0(t)$ along the beam shown in Fig. 3.2, the particular equilibrium solution is

$$\mathbf{s}_{\mathrm{p}}(x,t) = \begin{bmatrix} FL\xi_0\left(1-\xi_0\right)\left[1-\dfrac{\xi_0-\xi}{\xi^*}\right] \\ F\xi_0\left[\dfrac{1-\xi_0}{\xi^*}\right] \end{bmatrix} \tag{4}$$

where $\xi = x/L$, $\xi_0 = x_0(t)/L$, and

$$\xi^* = \begin{cases} \xi_0, & \xi \le \xi_0 \\ \xi_0 - 1, & \xi > \xi_0 \end{cases} \tag{5}$$

As a transverse load moves across the beam element, the position variable x_0 changes in time, thereby causing the section force vector to evolve in time. For brevity, the dependence on time will be dropped in the remaining derivation.

From the principle of virtual forces, compatibility between element and section deformations in the force-based formulation is expressed in integral form:

$$\mathbf{v} = \underbrace{\left(\int_0^L \mathbf{b}^T(x)\,\mathbf{f}_s(x)\,\mathbf{b}(x)\,dx \right)}_{\mathbf{f}} \mathbf{q} + \underbrace{\int_0^L \mathbf{b}^T(x)\,\mathbf{f}_s(x)\,\mathbf{s}_p(x)\,dx}_{\mathbf{v}_0} \tag{6}$$

where use of the linear-elastic section force-deformation relationship has been made. Numerical integration is applied to Eq. (6) since closed-form solutions are intractable for arbitrary functions $\mathbf{f}_s(x)$ and $\mathbf{s}_p(x)$, even for linear-elastic section response. As a result, the integrals in Eq. (6) become summations of N discrete function evaluations at locations $x_1, x_2, \ldots, x_N$ with associated integration weights $w_1, w_2, \ldots, w_N$

$$\mathbf{f} = \sum_{i=1}^{N} \mathbf{b}^T(x_i)\,\mathbf{f}_s(x_i)\,\mathbf{b}(x_i)\,w_i \tag{7}$$

$$\mathbf{v}_0 = \sum_{i=1}^{N} \mathbf{b}^T(x_i)\,\mathbf{f}_s(x_i)\,\mathbf{s}_p(x_i)\,w_i \tag{8}$$

For a nonprismatic beam element, the section flexibility matrix, $\mathbf{f}_s(x)$, contains irrational polynomials of x. As a result, there will be a numerical integration error in evaluating Eqs. (7) and (8) with quadrature rules that use simple monomials as basis functions, which is the case for the Gauss-Lobatto quadrature method (Abramowitz and Stegun 1972) typically applied to force-based elements. As the number of Gauss-Lobatto integration points increases, however, the integration error is reduced. Furthermore, the discontinuity of the first derivative of the internal bending moment produced by an interior transverse point load will lead to an additional numerical integration error in evaluating Eq. (8), regardless of the prismasticity of the element. These numerical integration errors will be of no consequence in computing the distribution of forces in a statically determinate structure; however, these errors will lead to discrepancies in the distribution of forces in an indeterminate structure since compatibility equations must be satisfied.

MOVING LOAD ANALYSIS OF A CANTILEVER

To demonstrate the numerical integration errors that arise in moving load analysis of non-prismatic beams, an analysis of a haunched cantilever is undertaken. Influence lines for internal force and nodal displacement of a statically determinate cantilever, as well as a statically indeterminate propped cantilever, are computed where a single force-based element represents the member. In each case, the computed response is compared to the response for a single displacement-based beam element with cubic Hermitian displacement functions (Cook *et al* 1989). As shown in Fig. 3.3, a unit load moves across the cantilever, which has the non-prismatic properties described by Brown (1984). Five-point Gauss-Lobatto integration is applied to evaluate all element integrals and only flexural deformations are considered in the analysis. Assuming a linear-elastic modulus of 200 GPa, the structural analyses are accomplished with the general purpose finite element algorithm OpenSEES developed by McKenna *et al* (2000).

Statically Determinate Cantilever

The finite-element solution of the problem provides a comparison between the force-based formulation, the displacement-based formulation and the closed-form exact solution. The fixed-end moment and free-end displacement are used as parameters for comparison with the closed-form exact solution. Fig. 3.4 illustrates results from the moving load analysis.

As shown in Fig. 3.4(a), the fixed-end moment from the force-based element is indistinguishable from the exact solution. The force-based formulation uses exact force interpolation functions between the element nodes. Consequently, irrespective of the nonprismatic geometry, the force-based element always presents the exact solution in statically determinate structures. In contrast to the force-based element, the displacement-based element presents a cubic variation in the fixed-end moment. The variation in the fixed-end moment is a direct result of the shape functions used in the element formulation.

Fig. 3.4(b) shows a comparison of the free-end displacement as a function of load position. The computed displacement from the force-based element is similar to the exact solution. It is a piecewise linear function, where the discontinuities are coincident with the integration points. As a result of the element compatibility relationship, numerical integration error appears in the computed displacement. Increasing the number of integration points ensures convergence to the exact solution. Fig. 3.4(b) also displays the computed displacement from the displacement-based element. The computed displacement is very similar to the exact solution. Even though the element provides a good approximation of the free-end displacement, it cannot approximate the fixed-end moment accurately. As a result, sufficient element discretization is necessary for the displacement-based element in moving load analysis.

Statically Indeterminate Propped Cantilever

Consider the cantilever beam shown in Fig. 3.3. A pin is applied to the free-end of the cantilever in order to create an indeterminate structure. The finite element response to the moving load is investigated by computing the fixed-end moment and propped-end rotation at each load step, as the load travels across the structure. For any given load step, other forces can be obtained from the equilibrium equation. The computed results are compared to the exact solution, which has been obtained using a finely discretized mesh consistent with finite element theory. The computed exact solution should provide an accurate approximation to the closed-form exact solution.

Fig. 3.5(a) and Fig. 3.5(b) shows variations in the fixed-end moment and propped-end rotation as functions of load position from the fixed end. Both the computed moment and the computed rotation from the force-based element are very close to the exact solution. The computed responses contain errors, which arise as a consequence of satisfying the element compatibility relationship. After satisfying the compatibility requirement, the errors are propagated along the element through the force interpolation functions. The computed results are in contrast to the previous example, where the computed moment is identical to the exact solution because the element only needs to satisfy equilibrium. In addition, the computed moment and rotation exhibit discontinuities coincident with the location of integration points in the force-based element. The discontinuities arise from extreme changes in the section shear force as the load moves across the integration points. Increasing the number of integration points will reduce errors associated with the element formulation and ensure convergence to the exact solution.

In comparison to the force-based element, the displacement-based element cannot provide a good approximation to the exact solution. Similar to the previous example, the displacement-based element displays cubic variations in the computed results because of the shape functions used in the formulation. Element discretization is necessary in order to provide a reasonable approximation to the exact solution.

Brown (1984) provides the exact solution for the case when the load is located at midspan. The solutions obtained using Just's full-stiffness matrix is used as a basis of comparison with the force-based element results. For simplicity, the bending moment and shear force at the fixed-end are used as parameters for comparison. Comparing the fixed end forces from the computed solution to a known solution demonstrates the accuracy of the force-based element. Furthermore, it provides justification for using force-based elements in moving load analyses.

When the load is applied at midspan, percent errors from the computed moment and shear are 7.58 % and 3.26 %, respectively. Increasing the number of integration points to nine reduces the percent errors to 0.96 % and 0.86 % for the computed moment and shear. The percent errors demonstrate convergence to the exact solution with increasing number of integration points, consistent with the element formulation.

The cantilever beam example demonstrates the capability of the force-based element to approximate the exact solution. Using sufficient number of integration points assures the accuracy of the computed response. In moving load analysis, errors in the computed solution are contributed from two sources. The numerical integration error associated with the element compatibility relationship and the discontinuity in the section shear force as the load moves across the integration points. These errors can be mitigated by increasing the number of integration points, which increases the accuracy of the computed solution.

The propped cantilever beam example demonstrates the force-based element's dependence on the geometry of the element. The force distribution along the element and nodal displacements are dependent of the nonprismatic geometry, location of integration points and associated weights. It is the consequence of the element compatibility relationship in the formulation. Approximating a continuous depth variation with discrete prismatic sections by numerical integration will instigate error in the finite element solution. Nevertheless, with sufficient number of integration points, the force-based element provides a good approximation to the exact solution as demonstrated in both examples.

SIMULATION OF FIELD MEASURED BRIDGE RESPONSE USING THE FORCE-BASED APPROACH

Kidarsa *et al* (2006) established a method to specify sections of interest on a bridge as integration points on the force-based element. The moving load analysis proves it is possible to obtain accurate results for the bridge forces using the Low Order Undetermined Coefficients integration method. The capability of the force-based element to simulate the response of nonprismatic structures in moving load analysis is presented in the following structural analysis. The Low Order integration method is implemented in the force-based formulation in order to obtain forces at sections of interest.

Consider the Seven Oaks Bridge, located on the Pacific Highway undercrossing at Seven Oaks interchange in Jackson County, Oregon (ODOT Bridge reference number 8539). A schematic of the bridge is shown in Appendix A. The bridge consists of two approach structures, and one main structure from span 3 to span 7.

The north approach spans are each 35 ft long from centerline of supports. The main structure consists of continuous nonprismatic reinforced concrete deck girders, with a quadratic variation in bottom flange width and constant depth. The south-most span is a 35 ft simple span. The spans support a roadway width of 30 ft, with a total width of 35 ft – 2 in.

There are four girder lines in each of the spans, with 8 in. x 52 in. diaphragms at quarter points. The girders are 12 in. x 54 in. uniform and prismatic along the approach structures. In the continuous spans of the main structure, the girders are 15 in. x 54 in. over the middle half of the spans; however, the bottom flange width tapers to 108 in. at continuous support locations. The bottom flange width variation in the first and last quarters of each span is shown Appendix A, and other pertinent dimensions are shown in Fig. 3.6. Using the specified concrete compressive strength of 22.8 MPa (3300 psi), the modulus of elasticity can be approximated as 22.6 GPa. Since the approach spans are independent structures with prismatic girders, only the main structure is considered in the finite element simulation.

The interior girder of the main structure represents the bridge stiffness variation along the span in the structural analysis. Each span is simulated with one force-based element, which accounts for variations in cross-section properties in the formulation. For simplicity, the horizontal curvature of the girder and the variation of girder centerline geometry are neglected in the analysis. Therefore, the interior girder is approximated as a straight girder.

The structure is subjected to a three-axle test truck traveling from the left support to the right support, as shown in Fig. 3.6. The test truck simulates an ODOT maintenance truck filled with gravel. The gross vehicle weight is 246 kN (55 kips) with a 67.4 kN steering axle and 179 kN tandem axle. The axle spacing between consecutive axles is approximately 4.37 m (172 in) and 1.40 m (55 in). Dynamic effects from truck movement are not included in the structural analysis because the wearing surface was smooth and the truck was applied at a crawl speed (8 mph) across the bridge.

The finite element analysis uses the Low Order Undetermined Coefficients integration rule with nine integration points in each force-based element. The integration points with constrained integration weights are assigned to locations that coincide with changes in stirrup spacing, determined from structural drawings. The remaining points are assigned to the middle of the span and other sections of interest. The undetermined weights are computed according to the formulation in

Kidarsa *et al* (2006). A list of integration points and weights are included in Table 3.1.

The moment and shear responses are used to evaluate the performance of the force-based element. A section of interest has been chosen to sample the moment and shear responses. It is located in span 5, approximately 4.78 m (15.69 ft) from the centerline of bent 5. The moment and shear force at the section of interest is compared to the moment and shear history obtained from the exact solution, as computed from a sufficiently refined finite element mesh of the bridge girders.

The error between the computed response and the exact solution is determined according to the definition

$$E(i) = \left| \frac{R(i) - R_{exact}(i)}{R_{\max}} \right| \times 100\% \qquad (9)$$

where i indicates the location as the load moves across the structure, R is the response ordinate, and R_{max} is the maximum absolute response of the exact solution. Scaling the absolute error by R_{max} rather than $R_{exact}(i)$ avoids spuriously large relative errors when the exact solution of the response ordinate approaches zero.

Computed results of the moving load analysis are presented in Fig. 3.7, where the computed moment and shear response at the section of interest are compared to the exact solution. As shown in the figure, the computed moment and shear response are nearly identical to the exact solution. Using equation (9), the maximum errors of the computed moment and shear response are determined to be 3.04% and 0.62%, respectively. Therefore, the computed response provides a good approximation to the exact solution.

Further assessment is facilitated by comparing the computed shear at the section of interest to the stirrup strain from experimental data. For analysis purposes, the section of interest is correlated to a test section on the bridge where experimental data is available (Higgins 2006). The test section is located in span 5, approximately 4.78 m (15.69 ft) from the centerline of bent 5. It represents a region experiencing relatively high live-load shear forces with diagonal cracks. Strain gages measure the stress carried by stirrups across diagonal cracks. The strain gages are installed by chipping into the concrete and exposing the embedded stirrup at the crack location. Typical installation of a strain gage is shown in Fig. 3.8.

Experimental data from the test section represent the stirrup strain recorded when the test truck moves across the bridge. The test truck is an ODOT maintenance truck filled with gravel, with axle weights and axle spacing similar to the test truck used in the finite element analysis. The data used for comparison with the force-based solution is obtained when the test truck travels westbound in the westbound lane at 8 mph (Fig. 3.9).

For a better comparison with experimental data, the integration points surrounding the test section are rearranged to capture the horizontal projection of the diagonal crack, as shown in Fig. 3.10. After computing the integration weights, the finite element analysis is repeated using the same moving truck load and bridge parameters. Computed results from sections crossing the diagonal crack are averaged for comparison with experimental data. The rearranged integration points and weights are presented in Table 3.2.

Since the shear force cannot be compared directly to the stirrup strain, each is normalized to its respective maximum absolute value. In addition, the domain of the experimental data is scaled and translated to the domain of the computed shear force. The objective of the assessment is to compare the locations of maximum and minimum values between computed results and experimental data. Assuming a proportionality constant and accounting for concrete contributions, the stirrup strain can be translated into section shear force.

In Fig. 3.11, the computed shear force at the section of interest is compared to the stirrup strain from experimental data. Fig. 3.11(a) displays the comparison when the shear force is computed using the original points and weights from Table 3.1; whereas, Fig. 3.11(b) displays the comparison when the shear force is computed using the rearranged points and weights in Table 3.2. In general, the computed shears from both figures appear similar.

The general shape of the computed shear appears similar to the shape of the experimental data, especially when the moving loads are located in the same span as the section of interest. Discontinuities in the experimental data coincide with discontinuities in the computed shear force. The locations of discontinuities indicate the instance when the truck axle travels across the section of interest. It proves the consistency between the computed response and experimental data. The similarity between computed shear force and experimental data is also observed by Higgins et al (2004) in an effort to assess the remaining life of reinforced concrete beams with diagonal cracks.

However, certain sections of the pseudo-time domain display a deviation between the computed shear and experimental data. The experimental data shows an opposite response to the computed shear. The discrepancy between computed results and experimental data is also observed by Higgins et al (2004). The difference is contributed by the dynamic nature of the experiment, the rigidity of the bent caps, distribution of loads to other girders, and shear contribution from concrete in the girder's compression zone.

Considering the uncertainties associated with bridge analysis, the slight difference between computed and experimental data demonstrates the force-based approach is an accurate and reliable approach to computing section forces on a structure subjected to moving loads. Moreover, the low-order integration rule allows a convenient method to specify critical sections as integration points within the force-based element.

CONCLUSION

The performance of the force-based element in moving load analyses of structures with nonprismatic members has been presented. Using exact force interpolation function, the force-based element satisfies strong equilibrium in the formulation. Only one force-based element is required to simulate the response of a nonprismatic structural member subjected to moving loads. The computed solution involves numerical integration error that can be reduced by increasing the number of integration points.

Applied to statically determinate structures, irrespective of the nonprismatic section dimensions, the force-based element provides identical results to the exact force distribution in the element. In addition, the computed displacements merely contain small errors associated with numerical integration. When applied to statically indeterminate structures, the force distribution in the element and nodal displacements are dependent on the nonprismatic geometry, location of integration points and associated weights. The element compatibility relationship becomes a function of the nonprismatic geometry.

The examples demonstrated the capability of the force-based element to approximate the exact solution. In addition, the low-order undetermined coefficient integration approach allows the specification of critical sections on the structure as integration points in the force-based element. Used in conjunction with the low-order integration approach, section forces at the critical locations can be determined from the integration points on the force-based element. Accurate section moment and shear from moving loads have been obtained using the new integration approach.

ACKNOWLEDGEMENT

This work was supported by the Oregon Department of Transportation, under grant umber MBMSFY04-041 awarded to Oregon State University. Their support is gratefully appreciated.

Notation

The following symbols are used in this paper:

$\mathbf{b}$ = section force interpolation matrix;

$\mathbf{e}$ = section deformation vector;

$\mathbf{f}_s$ = section flexibility matrix;

$\mathbf{k}_s$ = section stiffness matrix;

N = number of element integration points;

$\mathbf{q}$ = element basic force vector;

$\mathbf{s}$ = section force vector;

$\mathbf{s}_p$ = section force vector due to interior element loads;

$\mathbf{v}$ = element deformation vector;

w = integration point weight; and

x = integration point location.

References

Abramowitz, M. and Stegun, I. A. (1972). "Handbook of Mathematical Functions with Formulas, Graphs, and Mathematical Tables, 9th printing." Dover, New York, NY.

Baker, G. (1996). "Exact deflections in nonprismatic members." Journal of Computers and Structures, 61(3), 515 – 528.

Brown, C.J. (1984). "Approximate stiffness matrix for tapered beams." Journal of Structural Engineering, 110(12), 3050 – 3055.

Cook, R.D., Malkus, D.S., and Plesha, M.E. (1989). *Concepts and applications of finite element analysis*, 3rd ed., John Wiley and Sons, New York, NY.

El-Mezaini, N., Balkaya, C., Citipitioglu, E. (1991). "Analysis of frames with nonprismatic members." Journal of Structural Engineering, ASCE, 117(6), 1573 – 1592.

Filippou, F.C. and Fenves, G.L. (2004). "Methods of analysis for earthquake-resistant structures." *Earthquake engineering: From engineering seismology to performance-based engineering.* Y. Bozorgnia and V. V. Bertero, etd., Chap. 6, CRC, Boca Raton, FL.

Higgins, C., Yim, S.C., Miller, T.H., Robelo, M.J. and Potisuk, T. (2004). "Remaining life of reinforced concrete beams with diagonal-tension cracks." Report No. FHWA-OR-RD-04-12. <http://www.odot.state.or.us/tddresearch>.

Just, D.J. (1977). “Plane frameworks of tapering box and I-section.” Journal of the Structural Division, ASCE, Vol. 103, No. ST1, 71 – 86.

Kidarsa, A., Scott, M.H., Higgins, C.C. (2006). “Analysis of moving loads using force-based finite elements.” Submitted to the Journal of Structural Engineering in December, 2005, manuscript no. ST24937.

McKenna, F., Fenves, G.L, Scott, M.H., and Jeremić, B. (2000). “Open system for earthquake engineering simulation.” <http://opensees.berkeley.edu>.

Medwadowski, S.J. (1984). “Nonprismatic shear beams.” Journal of Structural Engineering, 110(5), 1067 – 1082.

Neuenhofer, A., and Filippou, F.C. (1997). “Evaluation of nonlinear frame finite-element models.” Journal of Structural Engineering, 123(7), 958 – 966.

Spacone, E., Ciampi, V., and Filippou, F.C. (1996). “Mixed formulation of nonlinear beam finite element.” Computers and Structures, 58, 71-83.

Tena-Colunga, A. (1996). “Stiffness formulation for nonprismatic beam elements.” Journal of Structural Engineering, 122(12), 1484 – 1489.

Zienkiewicz, O.C. and Taylor, R.L. (2000). *The finite element method: The basis*, 5th ed., Vol. 1, Butterworth, Stoneham, MA.

Span 3 and Span 7

Scaled to Domain [0,1]		Actual	
Points	Weights	Points (m)	Weights (m)
0.0	0.04	0.0	0.610
0.08	0.1	1.22	1.525
0.2	0.13	3.05	1.983
0.34	0.090885	5.185	1.386
0.5	0.278229	7.625	4.243
0.66	0.090885	10.065	1.386
0.8	0.13	12.20	1.983
0.92	0.1	14.03	1.525
1.0	0.04	15.25	0.610

Span 4 and Span 6

Scaled to Domain [0,1]		Actual	
Points	Weights	Points (m)	Weights (m)
0.0	0.043210	0.0	1.068
0.086420	0.086420	2.135	2.135
0.172840	0.098765	4.270	2.440
0.283951	0.118065	7.015	2.917
0.5	0.307080	12.353	7.586
0.716049	0.118065	17.690	2.917
0.827160	0.098765	20.435	2.440
0.913580	0.086420	22.570	2.135
1.0	0.043210	24.705	1.068

Span 5

Scaled to Domain [0,1]		Actual	
Points	Weights	Points (m)	Weights (m)
0.0	0.061322	0	1.627
0.122644	0.090172	3.254	2.393
0.180345	0.089080	4.785	2.364
0.300805	0.110731	7.982	2.938
0.5	0.297389	13.268	7.891
0.699195	0.110731	18.553	2.938
0.819655	0.089080	21.750	2.364
0.877356	0.090172	23.281	2.393
1.0	0.061322	26.535	1.627

Table 3.1. Location of points and weights of Seven Oaks Bridge.

Span 5

Scaled to Domain [0,1]		Actual	
Points	Weights	Points (m)	Weights (m)
0.051724	0.154483	1.372	4.099
0.157356	0.025862	4.175	0.686
0.203333	0.025862	5.395	0.686
0.300805	0.133842	7.982	3.551
0.5	0.319902	13.268	8.489
0.699195	0.133842	18.553	3.551
0.796667	0.025862	21.140	0.686
0.842644	0.025862	22.360	0.686
0.948276	0.154483	25.163	4.099

Table 3.2. Location of points and weights in span 5 of Seven Oaks Bridge after rearranging integration points around diagonal crack.

List of Figures

Basic System

$\mathbf{q} = [q_2 \;\; q_3]^T \qquad \mathbf{v} = [v_2 \;\; v_3]^T$

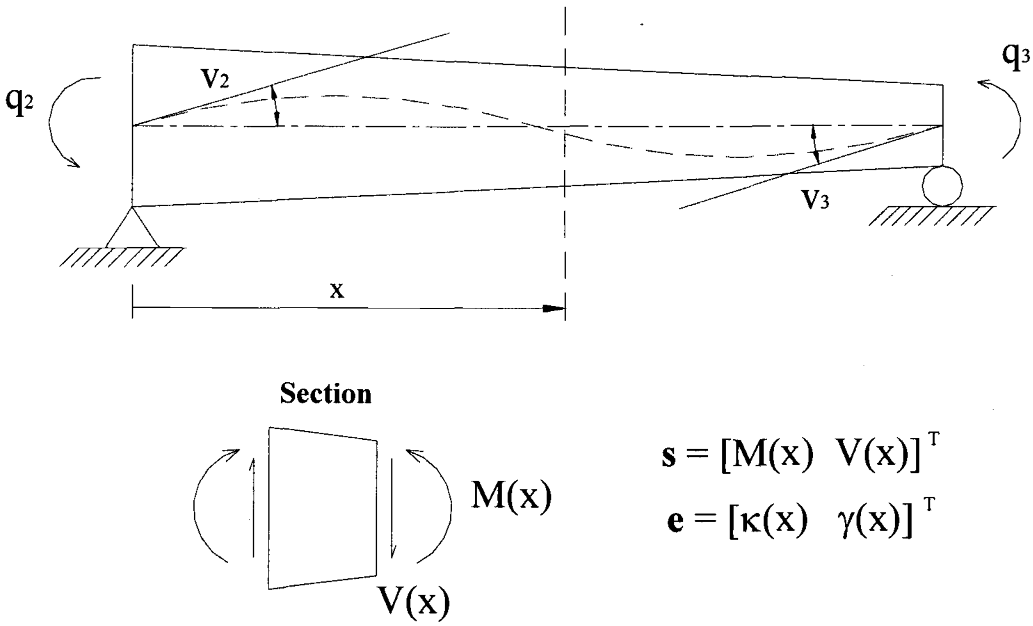

Figure 3.1. Simply-supported basic system and section forces for two-dimensional beam-column elements.

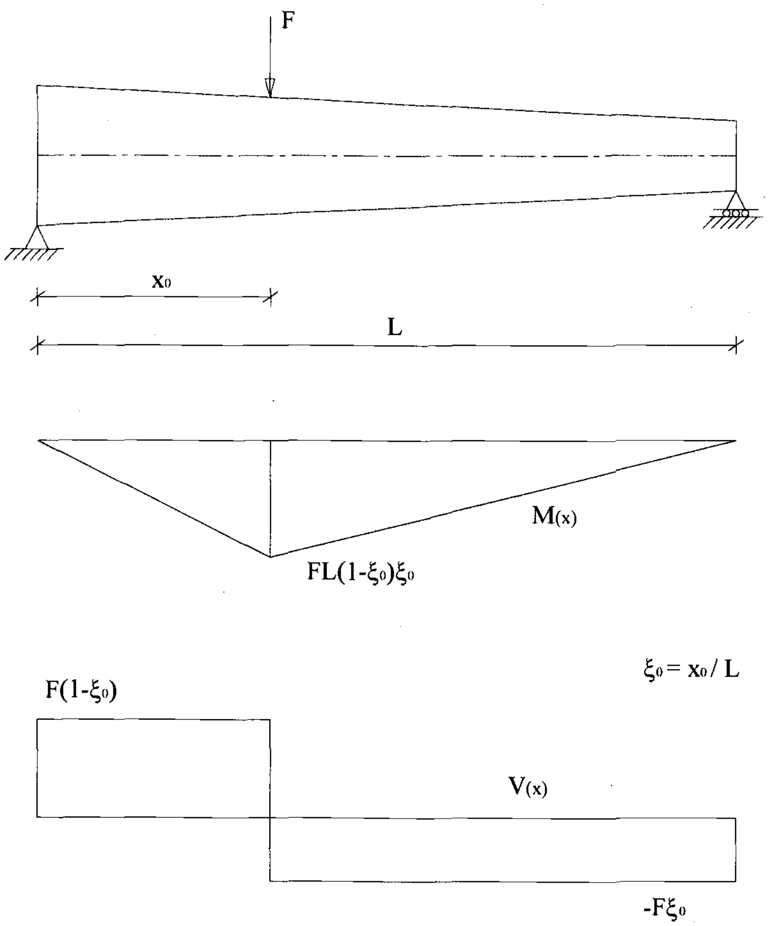

Figure 3.2. Bending moment and shear force developed in the simply-supported basic system for a transverse point load.

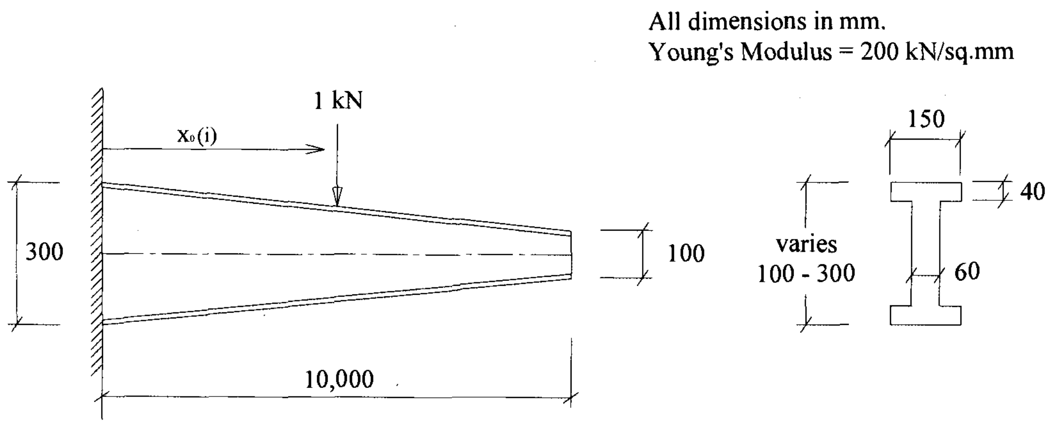

Figure 3.3. Nonprismatic cantilever beam with linearly varying depth and constant width.

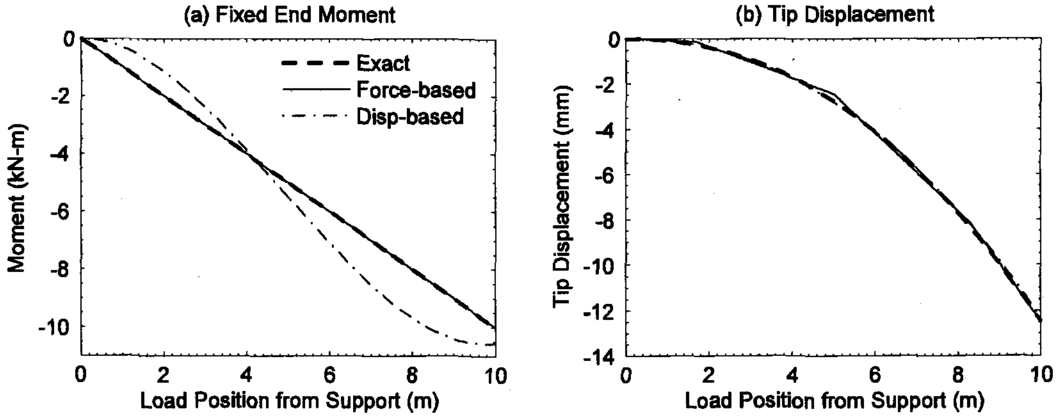

Figure 3.4. Comparison between computed and exact solution for nonprismatic cantilever beam example: (a) Moment at fixed end; and (b) Free-end displacement, as functions of load position.

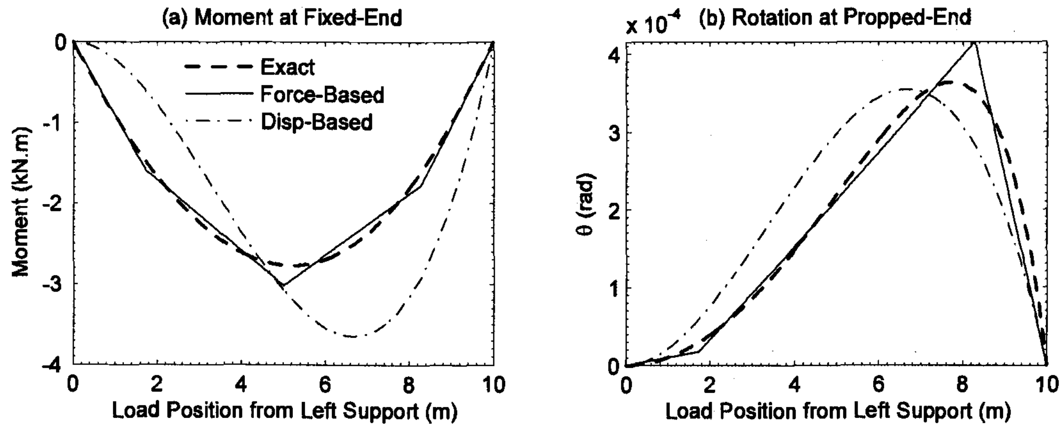

Figure 3.5. Comparison between computed and exact solution for propped cantilever beam example: (a) Moment at fixed-end; (b) Rotation at propped-end.

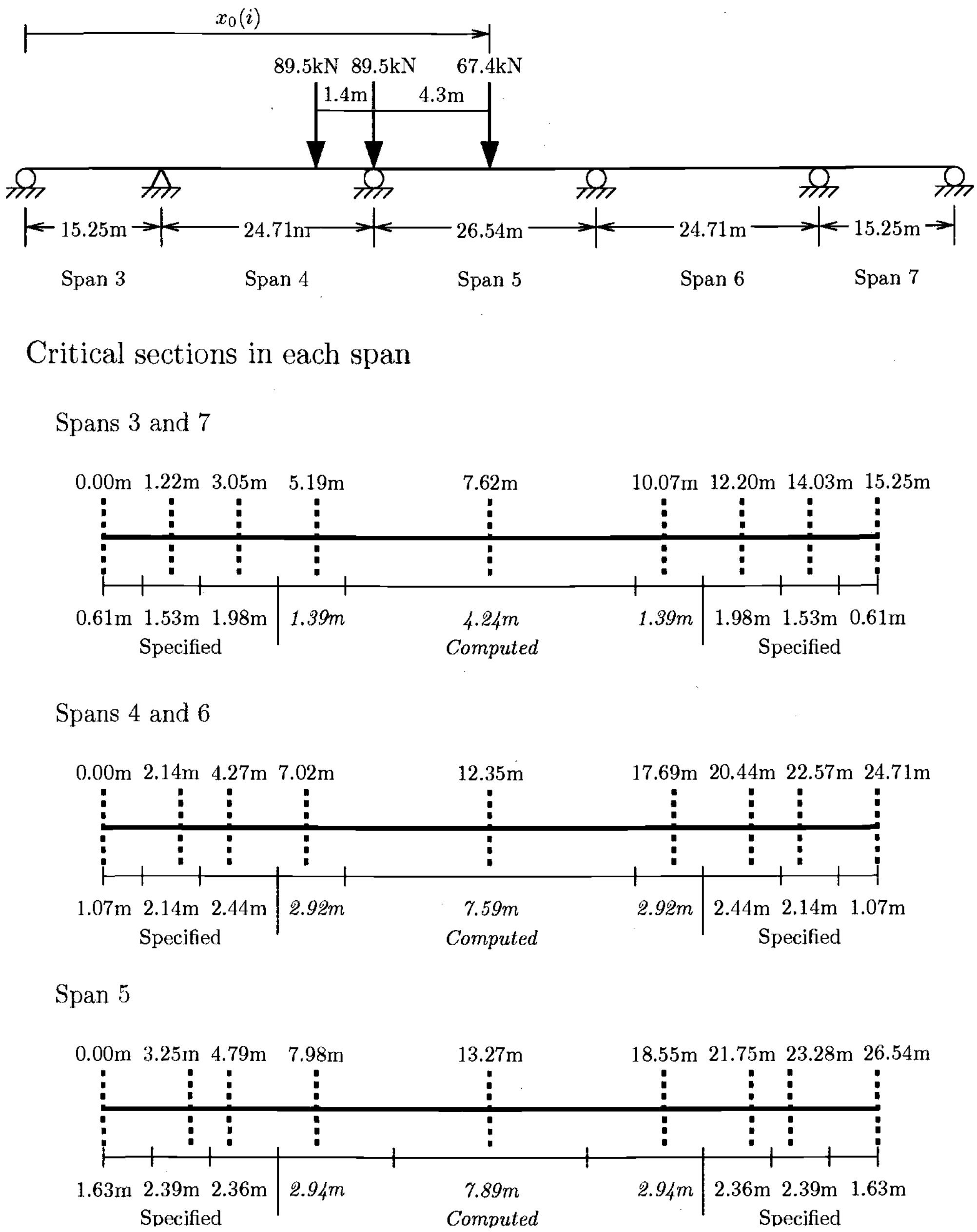

Figure 3.6. Model of Seven Oaks Bridge.

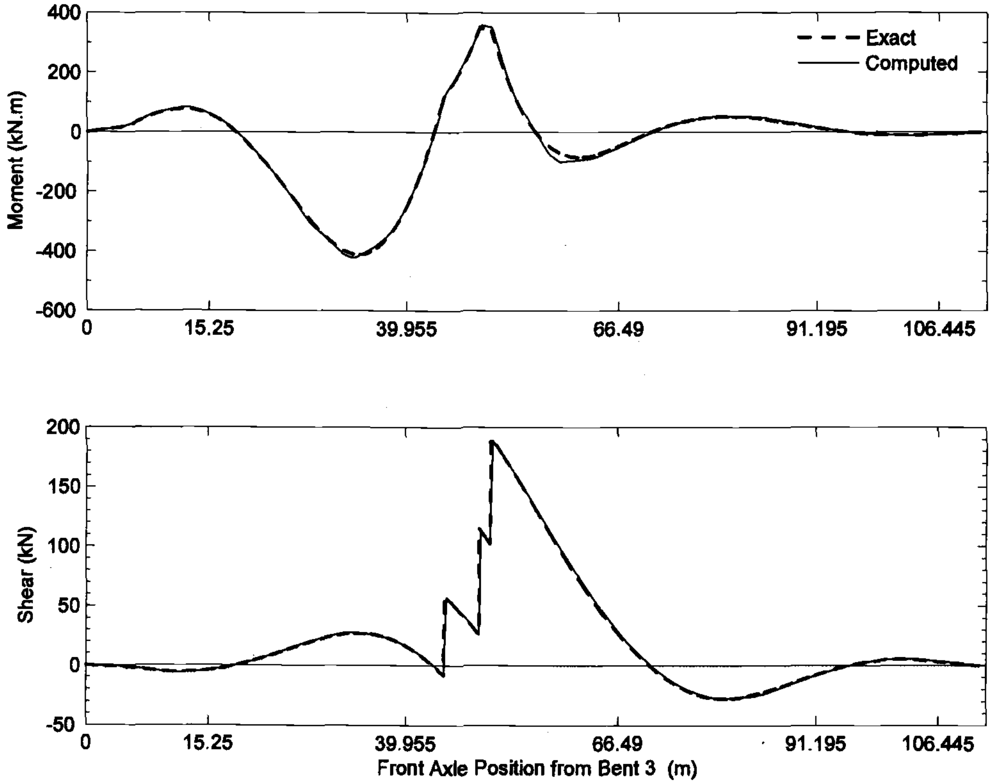

Figure 3.7. Seven Oaks Bridge moment and shear responses at section of interest from Finite Element Analysis.

(a) Test section at Seven Oaks Bridge

(b) Concrete removed to expose stirrup and attach strain gage

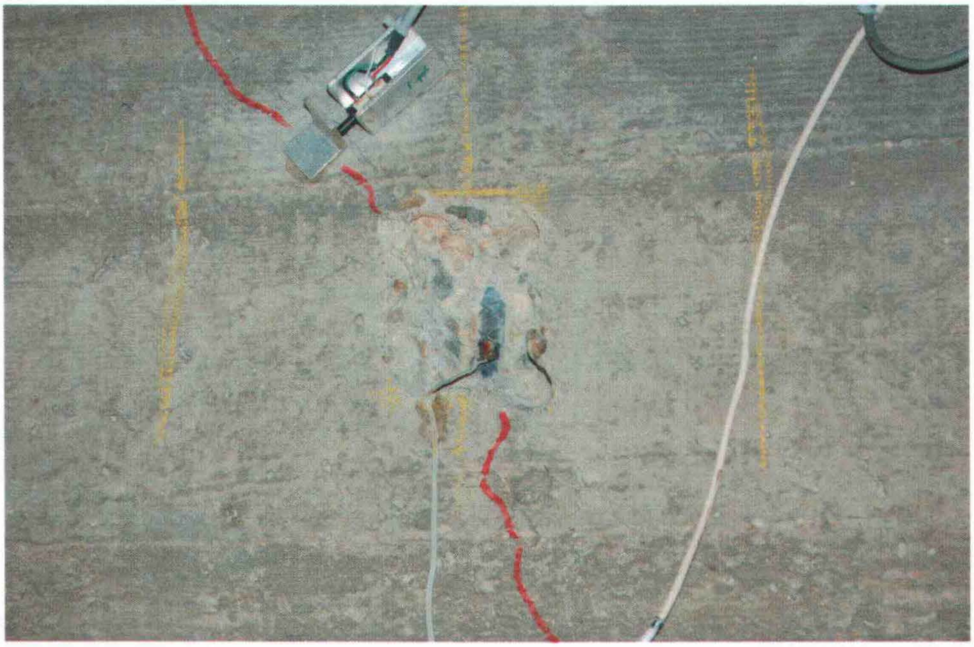

Figure 3.8. Instrumentation of Seven Oaks Bridge: (a) Test section at Seven Oaks Bridge; (b) Concrete removed to expose stirrup and attach strain gage.

Figure 3.9. ODOT maintenance truck traveling westbound in westbound lane at 8 mph.

Span 5

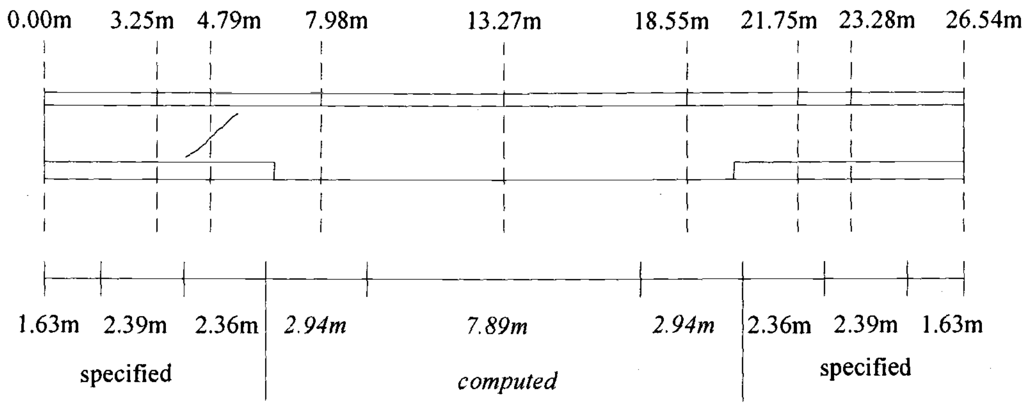

Original points and weights

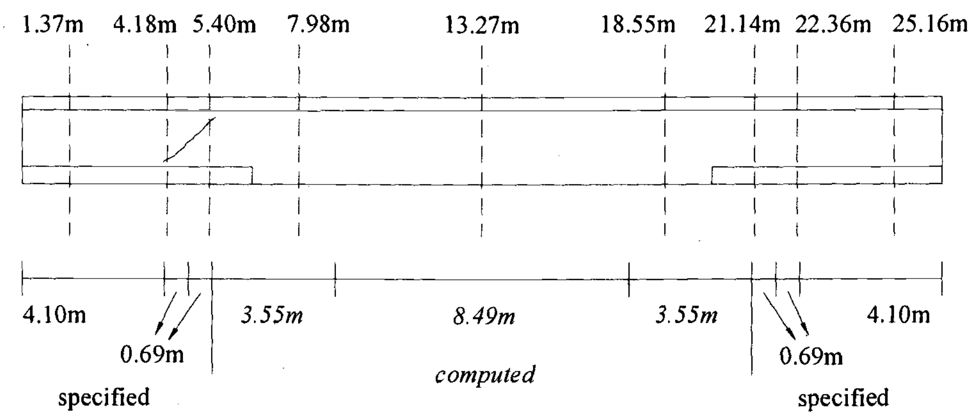

Rearranged points and corresponding weights

Figure 3.10. Comparison between original and rearranged location of integration points in span 5 of Seven Oaks Bridge.

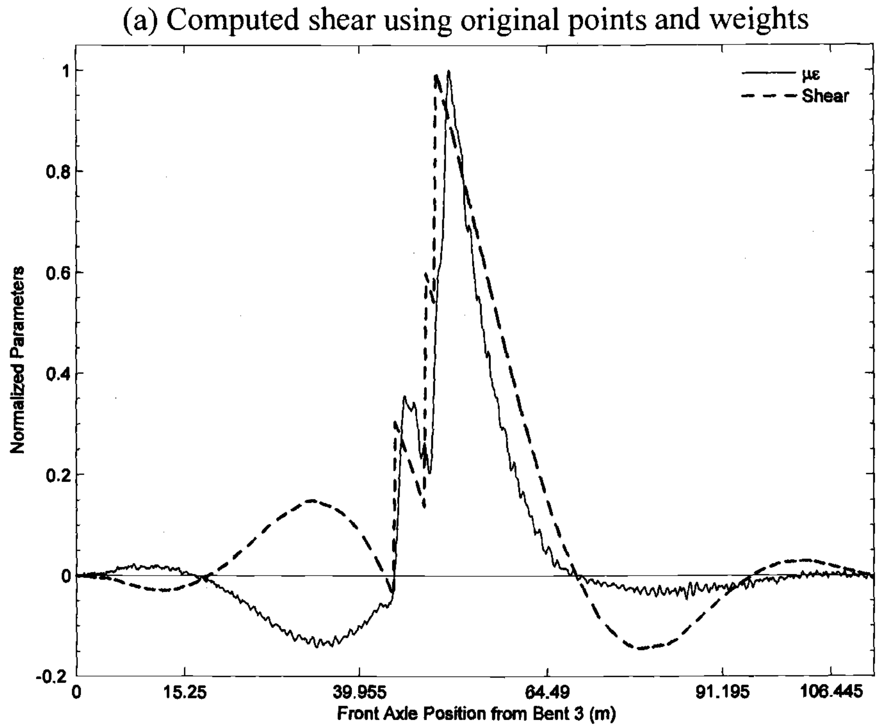

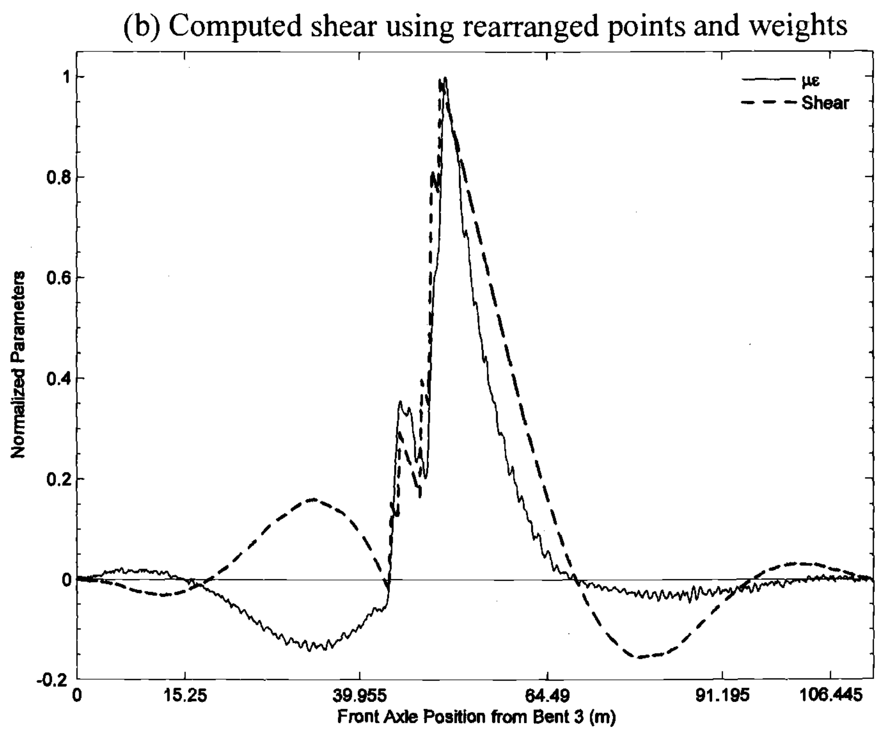

Figure 3.11. Comparison between computed shear and experimental data:
(a) Computed using original integration points; (b) Computed using redistributed integration points.

General Conclusion

Analyses of moving loads using the force-based finite element have been presented. Using exact force interpolation functions, the element satisfies strong equilibrium, therefore only one force-based element is required to simulate the response of a structural member to moving loads. Discretization of the finite element model is not necessary, even though additional critical locations are included in the analysis.

The first manuscript shows the force-based element can represent the exact solution in analyzing prismatic structures. In addition, the salient features of the force-based element are compared to the displacement-based based element. The second manuscript shows the force-based approach simulates well experimental data for structures with non-prismatic members subjected to moving loads.

A new numerical integration approach is introduced for the force-based formulation that allows critical locations in a structural member to be specified as the integration points of the element while maintaining an acceptable level of integration accuracy. Forces at the critical locations are determined by sampling forces at the integration points. Although the accuracy of this integration approach is of a low order, it is sufficient for practical applications in structural engineering. Analyses show the errors associated with the low order numerical integration are minor and accurate results for the internal forces at specified locations in a structure can be obtained using the force-based element in conjunction with this low order integration approach. In addition to moving load analysis, it is noted that low order integration has applications in representing the spread of plasticity (plastic hinges) in frame structures.

BIBLIOGRAPHY

AASHTO (1998). *LRFD bridge design specifications*, 2nd ed., American Association of State Highway and Transportation Officials, Washington, D.C.

Abramowitz, M. and Stegun, I. A. (1972). "Handbook of Mathematical Functions with Formulas, Graphs, and Mathematical Tables, 9th printing." Dover, New York, NY.

Baker, G. (1996). "Exact deflections in nonprismatic members." Journal of Computers and Structures, 61(3), 515 – 528.

Brown, C.J. (1984). "Approximate stiffness matrix for tapered beams." Journal of Structural Engineering, 110(12), 3050 – 3055.

Cook, R.D., Malkus, D.S., and Plesha, M.E. (1989). *Concepts and applications of finite element analysis*, 3rd ed., John Wiley and Sons, New York, NY.

El-Mezaini, N., Balkaya, C., Citipitioglu, E. (1991). "Analysis of frames with nonprismatic members." Journal of Structural Engineering, ASCE, 117(6), 1573 – 1592.

Filippou, F.C. and Fenves, G.L. (2004). "Methods of analysis for earthquake-resistant structures." *Earthquake engineering: From engineering seismology to performance-based engineering.* Y. Bozorgnia and V. V. Bertero, etd., Chap. 6, CRC, Boca Raton, FL.

Golub, G.H. and Van Loan C.F. (1996). *Matrix computations*, 3rd ed, The Johns Hopkins University Press, Baltimore, MD.

Higgins, C., Daniels, T.K., Rosowsky, D.V., Miller, T.H., and Yim, S.C. (2005). "Reliability based assessment of conventionally reinforced concrete bridges for shear." Journal of the Transportation Research Board, Approved for publication 2005.

Higgins, C., Yim, S.C., Miller, T.H., Robelo, M.J. and Potisuk, T. (2004). "Remaining life of reinforced concrete beams with diagonal-tension cracks." Report No. FHWA-OR-RD-04-12. <http://www.odot.state.or.us/tddresearch>.

Hughes, T.J.R. (1987). *The finite element method*, Prentice-Hall, Englewood Cliffs, NJ.

Just, D.J. (1977). "Plane frameworks of tapering box and I-section." Journal of the Structural Division, ASCE, Vol. 103, No. ST1, 71 – 86.

Kidarsa, A., Scott, M.H., Higgins, C.C. (2006). "Analysis of moving loads using force-based finite elements." Submitted to the Journal of Structural Engineering in December, 2005, manuscript no. ST24937.

Medwadowski, S.J. (1984). "Nonprismatic shear beams." Journal of Structural Engineering, 110(5), 1067 – 1082.

McKenna, F., Fenves, G.L, Scott, M.H., and Jeremić, B. (2000). "Open system for earthquake engineering simulation." <http://opensees.berkeley.edu>.

Neuenhofer, A., and Filippou, F.C. (1997). "Evaluation of nonlinear frame finite-element models." Journal of Structural Engineering, 123(7), 958 – 966.

Ranzo, G., and Petrangeli, M. (1998). "A fibre finite beam element with section shear modelling for seismic analysis of RC structures." Journal of Earthquake Engineering, 2(3), 443-473.

Scott, M.H., and Fenves, G.L. (2006) "Plastic hinge integration methods for force-based beam-column elements," Journal of Structural Engineering, 132(2).

Spacone, E., Ciampi, V., and Filippou, F.C. (1996). "Mixed formulation of nonlinear beam finite element." Computers and Structures, 58, 71-83.

Stoer, J., and Bulirsch, R. (1993). *Introduction to numerical analysis*, 2nd ed., Springer-Verlag, New York, NY.

Tena-Colunga, A. (1996). "Stiffness formulation for nonprismatic beam elements." Journal of Structural Engineering, 122(12), 1484 – 1489.

Zienkiewicz, O.C. and Taylor, R.L. (2000). *The finite element method: The basis*, 5th ed., Vol. 1, Butterworth, Stoneham, MA.

Appendices

Appendix A

Seven Oaks Bridge Drawings

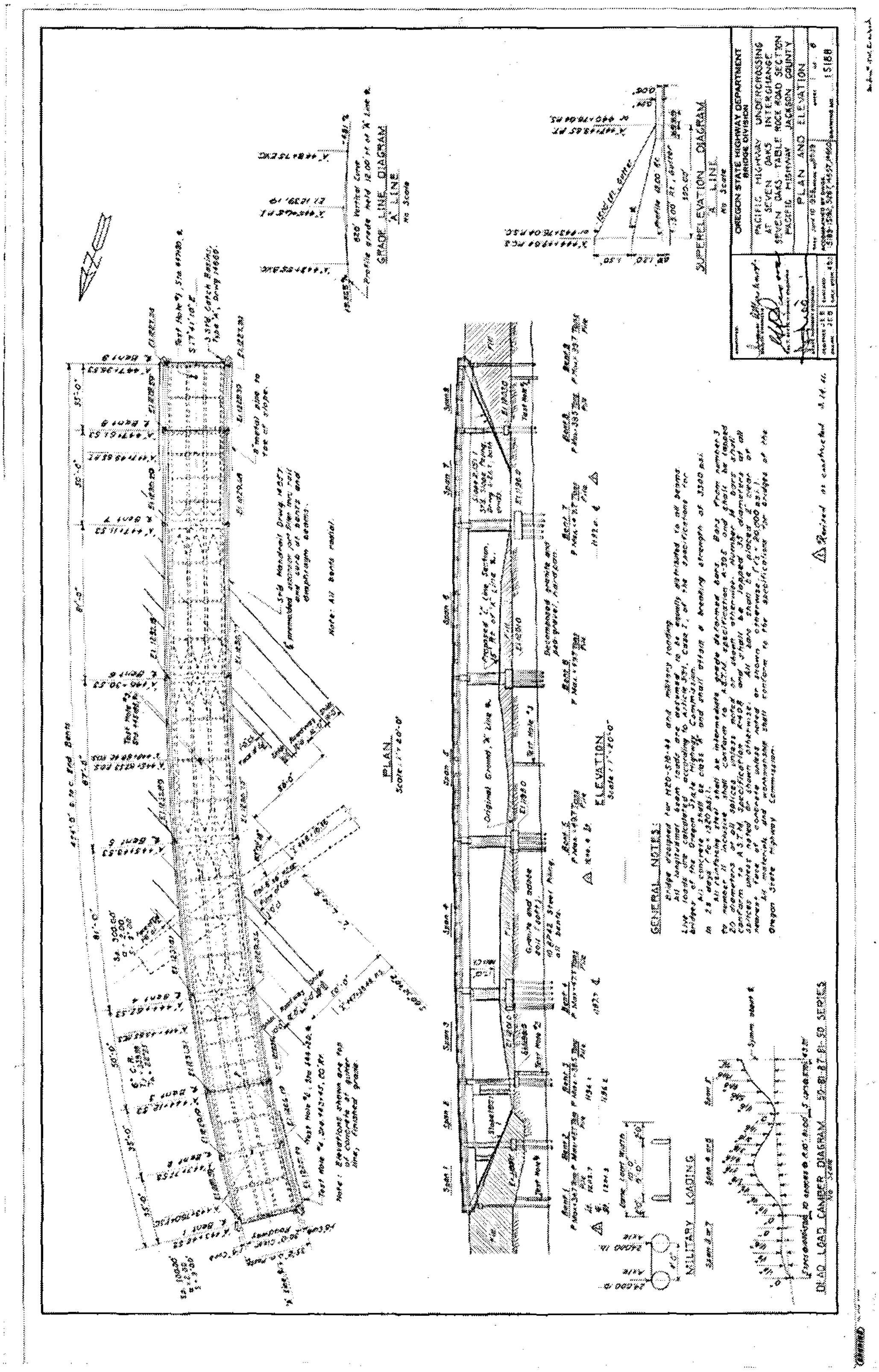

Drawing No. 15188: Seven Oaks Bridge plan and profile

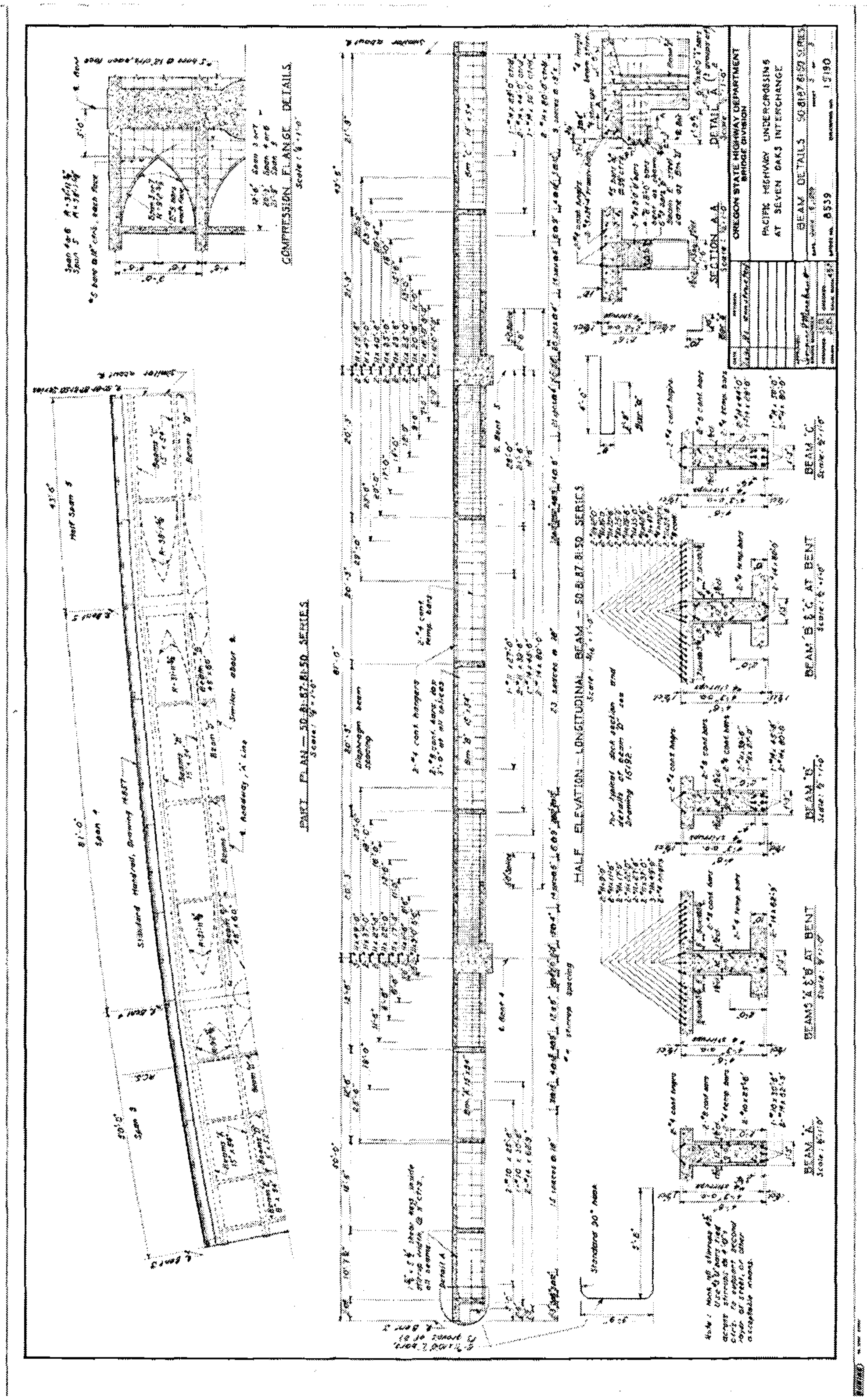

Drawing No. 15190: Seven Oaks Bridge beam details

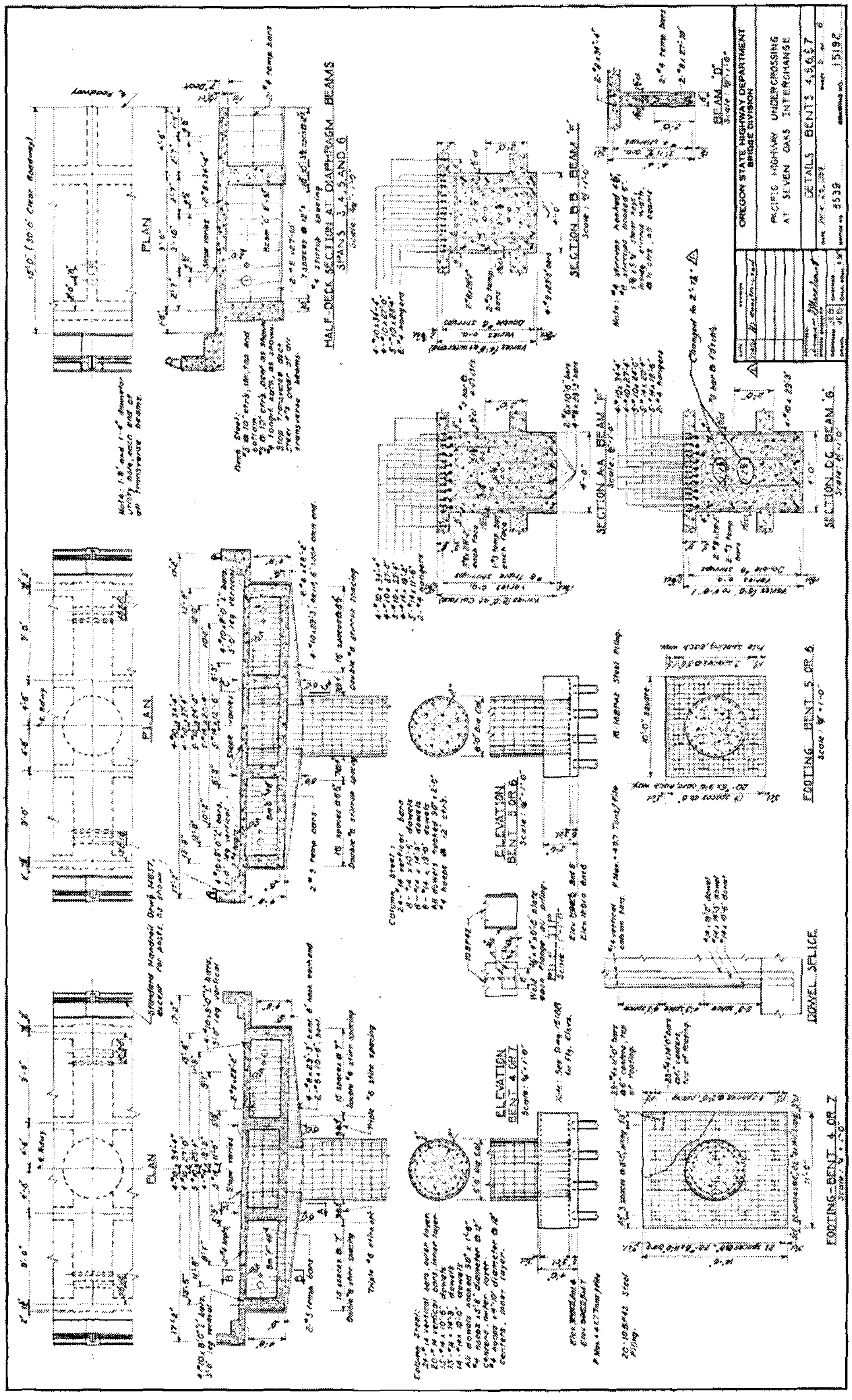

Drawing No.15192: Seven Oaks Bridge bent details